Results in Chemistry 18 (2025) 102769

Contents lists available at ScienceDirect

Results in Chemistry

journal homepage: www.sciencedirect.com/journal/results-in-chemistry

Performance optimization of CI engine using python with blends of waste oil biodiesel, plastic pyrolysis oil, and diesel

J. Mohammed Azarudeen [a], Anish Mariadhas [b,*], Jayaprabakar Jayaraman [b], S. Yashashwini [c], A. Vivek Anand [d], Karthick Muniyappan [e], Ankur Bahl [f], Mohammad Kanan [g,h,**], R. Muraliraja [i,*], Vimal Ramanathan [j]

[a] Research Scholar, School of Mechanical Engineering, Sathyabama Institute of Science and Technology, Jeppiar Nagar, Chennai, India
[b] School of Mechanical Engineering, Sathyabama Institute of Science and Technology, Jeppiar Nagar, Chennai, India
[c] Department of CSE, Cambridge Institute of Technology, Bengaluru, Karnataka 560036, India
[d] Department of Aeronautical Engineering, MLR Institute of Technology, Hyderabad, Telangana, India
[e] Department of Mechanical Engineering, Veltech Rangarajan Dr Sagunthala R&D Institute of Science and Technology, Chennai 600062, Tamil Nadu, India
[f] School of Mechanical Engineering, Lovely Professional University, India
[g] Department of Industrial Engineering, College of Engineering, University of Business and Technology, Jeddah 21448, Saudi Arabia
[h] Department of Mechanical Engineering, College of Engineering, Zarqa University, Zarqa, Jordan
[i] Department of Mechanical Engineering, Vels Institute of Science, Technology & Advanced Studies, Chennai 600 117, Tamil Nadu, India
[j] Faculty of Business & Communications, INTI International University, Putra Nilai, 71800, Malaysia

ARTICLE INFO

Keywords:
Waste plastic
Pyrolysis oil
Biodiesel

ABSTRACT

This study explores the novel integration of ternary fuel blends comprising diesel, biodiesel derived from waste cooking oil, and pyrolysis oil obtained from waste plastics in a single-cylinder direct injection compression ignition (CI) engine. A major innovation lies in the simultaneous utilization of two waste-derived fuels—biodiesel and plastic pyrolysis oil—to create a sustainable, low-emission alternative to conventional diesel. Engine tests were conducted under varying injection pressures (170, 200, and 230 bar) and load conditions to evaluate brake thermal efficiency (BTE), exhaust gas temperature (EGT), and key emissions such as NOx, CO, UHC, and smoke opacity. The results indicate that blends such as P10B220D70 and P15B215D70 offer optimal engine performance and combustion stability at 230 bar injection pressure. Notably, a Python-based statistical correlation analysis was employed to determine the influence of input variables (fuel blend, injection pressure, and load) on engine performance and emissions, identifying injection pressure as the most significant factor. This integrated experimental and computational approach underscores the viability of ternary waste-fuel blends as a promising solution for cleaner and more efficient CI engine operation.

1. Introduction

Diesel engines are extensively employed for transforming chemical energy into mechanical output, primarily due to their high efficiency, dependable operation, and adaptability across a wide spectrum of applications [1–3]. In the face of escalating global energy needs and declining fossil fuel reserves, identifying renewable and eco-friendly fuel alternatives has become crucial for ensuring long-term energy stability and minimizing ecological degradation [4,5]. Biodiesel, typically produced from vegetable oils and animal-based fats, has been a major area of investigation as a replacement for conventional diesel [6,7,8]. In recent years, novel sources such as microalgae have gained attention for their potential to serve as carbon-neutral biofuels. Simultaneously, the growing accumulation of plastic waste presents serious environmental and health concerns, including soil and water pollution, toxicity risks, and heightened fire hazards [9–11]. It is estimated that the world discards over a billion used tires each year [9], intensifying the urgency to repurpose these materials. One such method is pyrolysis—a thermal decomposition technique conducted in an inert (oxygen-free) atmosphere. This process breaks down waste materials into valuable byproducts such as pyrolysis oil, combustible gases, solid char, and recyclable steel wire [12]. Among these, pyrolysis oil has emerged as a promising alternative fuel for diesel engines [13,14], aligning with both

* Corresponding authors.
** Co-corresponding author.
E-mail addresses: anish2010me@gmail.com (A. Mariadhas), yashaswini.cse@cambridge.edu.in (S. Yashashwini), muralimechraja.se@vistas.ac.in (R. Muraliraja).

https://doi.org/10.1016/j.rechem.2025.102769
Received 6 June 2025; Accepted 3 October 2025
Available online 10 October 2025

Nomenclature

P	Pyrolysis oil derived from plastic waste (WPO), % by volume
B1/B2/B3	Biodiesel derived from Waste Cooking Oil (WCO), from batch 1/2/3, % by vol.
D	Conventional petroleum diesel, % by volume
P10B120D70	10 % WPO + 20 % WCO Biodiesel (Batch 1) + 70 % Diesel
P15B115D70	15 % WPO + 15 % WCO Biodiesel (Batch 1) + 70 % Diesel
P5B125D70	5 % WPO + 25 % WCO Biodiesel (Batch 1) + 70 % Diesel
P10B220D70	10 % WPO + 20 % WCO Biodiesel (Batch 2) + 70 % Diesel
P15B215D70	15 % WPO + 15 % WCO Biodiesel (Batch 2) + 70 % Diesel
P5B225D70	5 % WPO + 25 % WCO Biodiesel (Batch 2) + 70 % Diesel
P10B320D70	10 % WPO + 20 % WCO Biodiesel (Batch 3) + 70 % Diesel
P15B315D70	15 % WPO + 15 % WCO Biodiesel (Batch 3) + 70 % Diesel
P5B325D70	5 % WPO + 25 % WCO Biodiesel (Batch 3) + 70 % Diesel|

monoxide emissions under optimized engine conditions. Seljak et al. [17] demonstrated that TPO performs effectively in turbocharged diesel engines without intercoolers, especially at higher load operations. Koc and Abdullah [18] explored ternary fuel mixtures comprising 10 % tire oil, biodiesel, and 80 % diesel, finding that this combination enhanced torque and power output, improved fuel efficiency, and lowered emissions of nitrogen oxides and carbon monoxide compared to binary blends. Meanwhile, waste plastic oil (WPO) has emerged as another promising diesel substitute. Sanyal et al. [19] observed that increasing the WPO proportion in fuel blends led to elevated emissions, primarily due to the oil's higher viscosity and aromatic content. However, incorporating 10 % n-butanol effectively reduced NOx emissions [20]. Additionally, optimizing injection timing and employing exhaust gas recirculation (EGR) techniques contributed to improved thermal efficiency and reduced smoke and NOx formation [21]. Sambandam et al. [22] found that the addition of 10 % 2-methoxy ethyl acetate to diesel-WPO blends enhanced brake thermal efficiency while lowering emissions, whereas Kharkwal et al. [23] reported that introducing 5–10 % diethyl ether helped decrease smoke and carbon emissions from waste cooking oil blends. In contrast, Kumar et al. [24] noted an increase in smoke emissions when using WPO fuels, attributing this to the unique physical and chemical properties of the blends.

Injection pressure plays a pivotal role in governing combustion efficiency and emission profiles in compression ignition engines fueled with biodiesel and waste-derived blends. Higher injection pressures typically promote better atomization and fuel–air mixing, thus enhancing combustion quality and reducing incomplete combustion products. Simultaneously, the widespread accumulation of non-

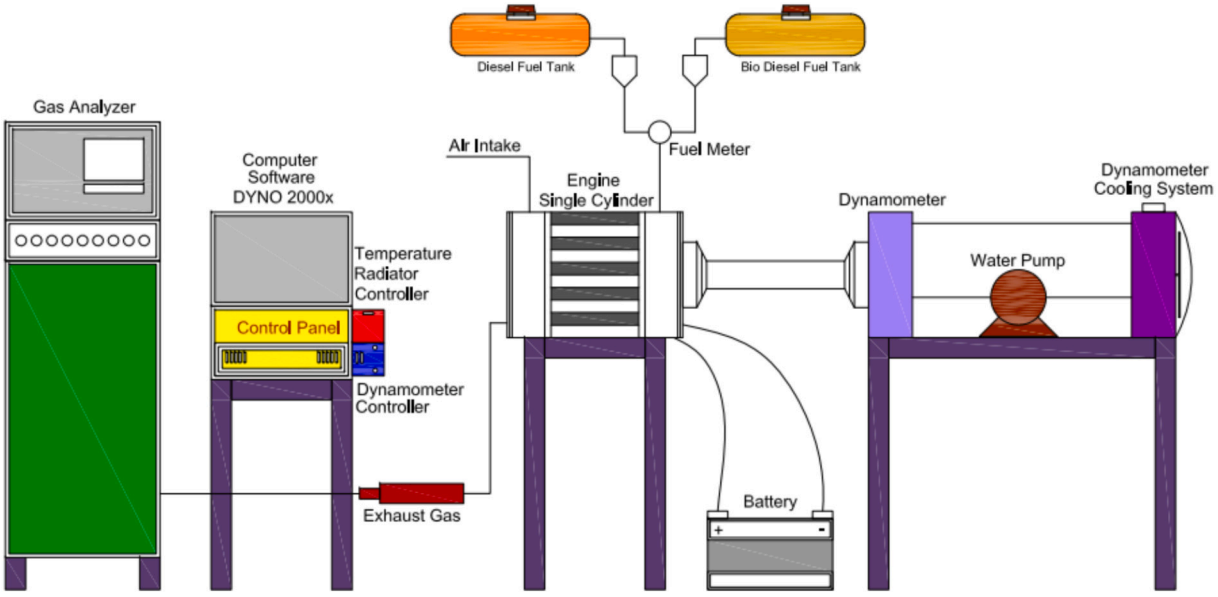

Fig. 1. Trial Setup Layout.

sustainable energy goals and integrated waste reduction strategies. Its utilization not only offers a path toward cleaner combustion but also supports circular economy principles by converting non-biodegradable waste into usable energy resources.

Numerous studies have investigated the potential of tire pyrolysis oil (TPO) as an alternative fuel for diesel engines. Vel Murugan et al. [15] evaluated blends containing 10 %, 30 %, and 50 % TPO with conventional diesel in a single-cylinder engine and concluded that TPO shows significant promise for future diesel-powered energy systems. Sharma and Murugan [16] examined an 80 % biodiesel and 20 % TPO blend, reporting substantial reductions in hydrocarbon, smoke, and carbon

biodegradable plastics presents a serious ecological challenge. Pyrolysis, a thermochemical process performed in the absence of oxygen, offers a viable method for converting plastic waste into pyrolysis oil—a combustible fuel compatible with diesel engines [25]. Integrating WCO-derived biodiesel with waste plastic pyrolysis oil (WPO) into ternary blends with diesel not only addresses waste disposal issues but also supports circular economy principles and energy recovery efforts. Several studies have demonstrated the feasibility of using tire or plastic-derived pyrolysis oils in CI engines. Sharma and Murugan [26] observed a 24 % reduction in CO and 19 % reduction in HC when 20 % TPO was blended with 80 % biodiesel. Similarly, Vallapudi et al. [27] reported

Table 1
Test engine standards.

Feature	Specification
Cylinder Dimensions	85.1 mm (bore) × 120 mm (stroke)
Total Displacement	654 cc
Injector Orifices	4 holes
Orifice Diameter	0.25 mm
Fuel Spray Angle	130°
Injection Start Timing	21° before TDC (bTDC)
Crown Geometry	Toroidal piston bowl
Cylinder Dimensions	87 mm (bore) × 110 mm (stroke)
Total Displacement	654 cc

Fig. 2. Pictorial depiction of the Engine.

Table 2
Hallmarks of pressurized transducer.

Design/model	KISTLER-7031
Pressure Accuracy	±0.2 bar
Physical Dimensions	Diameter: 10.2 mm
Natural Resonance Frequency	75 kHz
Pressure Measurement Range	0 to 300 bar
Temperature Operating Limits	Minimum: −40 °C
Charge Sensitivity	60 pC/bar

that tamarind seed methyl ester blends at 220 bar injection pressure led to a 6 % improvement in BTE and 16 % lower smoke emissions. Yesilyurt [28] found that WCO biodiesel blends at 210 bar improved combustion characteristics while reducing CO by 22 %, HC by 18 %, and smoke by 25 % compared to diesel. These findings affirm the performance and emission benefits of biodiesel-based ternary blends. Injection pressure is another critical variable that strongly influences combustion dynamics. Increasing injection pressure enhances fuel atomization, leading to better air–fuel mixing, reduced ignition delay, and more complete combustion. Saravanan et al. [29] found that raising injection pressure from 200 to 240 bar resulted in a 4.8 % increase in BTE and 27 % reduction in CO emissions. Srivastava et al. [30] demonstrated that dual-fuel CI engines with acetylene and elevated injection pressures achieved up to 10.5 % BTE improvement. Altun et al. [31] confirmed that a blend of 15 % propanol and 85 % diesel at 220 bar led to 12 % NOx reduction and better peak cylinder pressure.

Despite these advancements, a systematic approach evaluating both ternary waste-fuel blends and injection pressure modulation is lacking. Most prior studies focus on binary fuel systems or single injection settings, limiting optimization potential. This study addresses this gap by investigating the combustion, performance, and emission characteristics of ternary blends composed of waste cooking oil biodiesel, plastic pyrolysis oil, and diesel, under three injection pressures (170, 200, and 230 bar). A modified single-cylinder, four-stroke CI engine was used to conduct the experiments across varying engine loads. Additionally, Python-based statistical modeling was applied to correlate input variables with output performance, offering a novel computational insight into engine behavior. This integrated experimental-computational study aims to determine optimal fuel blends and injection conditions for enhanced thermal efficiency, lower emissions, and sustainable CI engine operation using waste-derived fuels.

In this study, Python was employed as a robust analytical tool to process and interpret experimental engine data for performance optimization. The input parameters fuel blend type (A), injection pressure (B), and engine load (C) were systematically mapped against key output responses such as brake thermal efficiency (BTE), brake specific energy consumption (BSEC), cylinder pressure, exhaust gas temperature (EGT), and emissions (CO, HC, NOx, smoke opacity). Using Python libraries like pandas, numpy, and seaborn, a correlation matrix was computed to determine the strength and direction of linear relationships between variables. This matrix helped identify injection pressure as the dominant factor influencing engine performance and emissions. These insights guided the selection of optimal operating conditions (particularly 230 bar injection pressure) and blend ratios (notably P10B220D70), thus enabling a data-driven approach to optimize CI engine performance using waste-derived fuels.

2. Investigation framework

An exploratory analysis was investigated using a Kirloskar uni-cylinder, four-stroked direct load diesel engine, as illustrated in Fig. 1. Operating steadily at 1500 rpm, it produces approximately 4.4 kW power. The engine features an 85.2 mm bore, 120 mm stroke, and 18.4:1 compression ratio. Injection timing and pressure are preset at 23° bTDC and 200 bar, respectively (Table 1). (See Fig. 2.)

3. Diagnostic and recording systems

To capture the in-cylinder load and calculate the heat exhaustive rate (HRR) during engine operation, a Kistler pressured sensor alongside a MICO fuelled injector are mounted on the cylindered head. Table 2 provides a comprehensive overview of the pressure sensor's operability details. Emission levels of CO, HC, and NOx are precisely measured using a QRO-402 exhaust gas analyzer, while smoke opacity is assessed with an AVL 437C smoke meter. Engine load control is achieved through an eddy ampered dynamometer, which is elastically coupled to the tested engine. Loaded adjustments are made in 25 % steps, ranging from idle (0 %) to full load (100 %), by varying the dynamometer ampere. SAE40 lubricating oil is utilized to minimize friction among the engine's moving parts during testing.

3.1. Components influencing engine response

Electromagnets connected to rotors that are firmly fixed to the crankshaft assembly are used in the dynamometer used for power quantification. Variations in the induced current take place as the rotor revolves inside the electromagnetic field produced by the coils. Changing

causes a varied load on the engine by gradually increasing the electromagnetic braking torque delivered to the rotor. Using a strain gauge sensor, torque (T) is calculated by multiplying the reactive force (F) by the moment arm length (R) concerning the pivot axis of the strain gauge, as defined in identity (1). This disposition permits the strain gauge to capture load-impacted strain variations resulting from the dynamometer's counteracting force. After torque measurement, brake power (BP) is derived under the condition of a constant angular velocity (N) of the engine.

$$T = F\,xR\ (N) \tag{1}$$

$$BP = 2\,\pi NTS/60\ (kW) \tag{2}$$

The symbol 'S' represents the dynamometer calibration constant.

Table 3
Assertions of exhaustive gas analyzer.

Design/model	QROTECH, Korea (QRO-400)
Correctness	± 0.01 % CO, ± 0.02 % CO_2 ± 25 ppm HC, ± 15 ppm NO_x
Proportions	280 mm × 400 mm × 150 mm
Load	4.1 kg
Proportions	< ± 2 % of Full-scaled reading
Category Heating range	0–30 °C
Accuracy	NDIR make (CO/CO_2 / HC) Electrochemical scale (O_2 / NO)
Sample requirement	4–6 lpm
Response time	< 10 s
Reheating time	2–8 min
Power supply	45 W

Table 4
Rating of smoky meter.

Design/model	AVL, Australia (AVL-436C-IP-50)
Measurement Assembly Length	0.47 m ± 0.007 m El
Illumination Source	6 W / 24 V Quartz Halogen Lamp
Electrical Input Requirements	210–250 V AC
Device Dimensions (L × W × H)	600 mm × 520 mm × 1300 mm
Opacity Detection Range	0–100 % opacity
Pre-Measurement Warm-Up Time	15 min
Maximum Smoke Heating Capacity	< 230 °C
Measurement Precision	±0.08 HSU

Table. 5
Precis of evaluated uncertainties.

Parameter	Percentage uncertainties
Brake Power (BP)	± 0.45
Fuel Flow Rate	± 0.18
Applied Load Measurement	± 0.38
Total Fuel Consumption	± 10.5
Load Response (Pickup)	± 11.0
Engine Speed	± 0.22
Temperature Range	± 0.28
Hydrocarbon (HC) Emissions	± 0.18
Carbon Monoxide (CO) Emissions	± 0.17
Nitric Oxide (NO_x) Emissions	± 0.27
Smoke Opacity	± 0.75
Overall Combined Uncertainty	2.08

Braking power (BP) is computed via Eq. (2), considering load variations spanning from 0 % to full scale (100 %) while maintaining a steady engine speed of 1500 rpm. Fuel consumption rates are determined by timing the interval required for the engine to utilize a precise fuel quantity of 10 cm^3, employing a stopper clock, as formulated in Eq. (3).

$$TFC = \rho x V/t\ (g/s) \tag{3}$$

In this context, TFC signifies the overall fuel consumption, 'ρ' indicates the density of the fuel, 'v' represents the measured fuelled volume, and 't' corresponds to the elapsed time asserted by the stopper clock for the depletion of 10 cm^3 of fuel. Leveraging the values of TFC and BP, the brake specific fuelled consumption (BSFC) is derived. Additionally, the brake thermal efficacy (BTE) is evaluated according to the formulation provided in Eq. (4).

$$BTE = (BP/TFCxCV)*100\% \tag{4}$$

The parameter 'CV' signifies the specific energy content (calorific value) of the fuel under investigation. Airflow rate entering the engine is quantified with high precision via a U-tubed manometer system featuring an orificer plate of roughly 20 mm diameter. The volumetric air flow rate (VA) is derived by applying the formula outlined in Eq. (5), accounting for differential pressure and fluid dynamics principles.

$$V_A = C_d x A x \sqrt{(2gH)}\ (m^3) \tag{5}$$

In this context, 'C_d' corresponds to the discharging coefficient, assigned a numerical of 0.62. The symbol 'A' indicates the orifice's cross-sectional space expressed in square meters (m^2). 'H' represents the differential head of the water depth measured in meters (m), while 'g' denotes the gravitational accelerating constant, quantified in meters per second squared (m/s^2).

3.2. Emission output topology

In-cylinder pressure measurements were taken with a KISTLER 7031 piezoelectric pressure transducer, which was calibrated before testing using a dead-weight piston calibration rig (Kistler Type 2893 A) following ISO 17025 standards. Torque and engine speed were recorded using an AVL 436C strain-gauge dynamometer system, with real-time data acquisition handled by a National Instruments DAQ card. The dynamometer's load cell was calibrated using standardized weights, while the speed sensor was verified with a Lutron DT-2234B handheld optical tachometer. Fuel flow rate was measured gravimetrically using a Class A 50 mL graduated glass burette, with cross-verification performed on a Shimadzu AUW220D precision balance (±0.1 mg sensitivity). The stopwatch used for timing fuel consumption was calibrated against a NABL-certified Traceable Digital Timer to ensure accuracy. Carbon monoxide (CO) and hydrocarbons (HC) emissions were measured using the QRO-400 analyzer (QROTECH), which employs nondispersive infrared (NDIR) technology with detection ranges of 0–9.99 % vol for CO and 0–1500 ppm for HC. Nitrogen oxides (NOx) were monitored using electrochemical sensors covering 0–500 ppm. Smoke opacity was evaluated via an AVL 437C photoelectric smoke meter (IP-52), calibrated from 0 to 100 %. Detailed instrument specifications appear in Tables 3 and 4. Emission results are normalized as grams per kilowatt-hour (g/kWh) to accurately assess engine performance and environmental impact. The QROTECH QRO-400 exhaust gas analyzer was calibrated before every measurement session using certified span and zero gases with the following concentrations: CO (0.5 %), CO_2 (10 %), NOx (200 ppm), and HC (500 ppm). The device uses non-dispersive infrared (NDIR) and electrochemical cell methods for analysis. Calibration followed the strict requirements of the USEPA Protocol Gas Verification standards.For smoke measurements, the AVL 437C IP-52 smoke meter was calibrated using a zero filter (clean ambient air) and a span filter (an opacity reference standard). The calibration process complied with ISO 11614 guidelines, as specified by the manufacturer.

3.3. Integrated experimental uncertainty model

The baseline output readings of the measurement instruments were utilized to assess the maximum conceivable uncertainties associated with various observed parameters, including voltage, current, temperature, and time. Subsequent error propagation analyses were conducted to quantify inaccuracies in derived quantities such as fuel consumption rate, applied load, and blood pressure. The percentage uncertainties corresponding to these parameters are compiled in Table 5. These error estimations were derived by integrating the minimum measurable values with the specified instrument precision. Given that a calculated variable "S" is a function of multiple independent inputs (x_1, x_2, x_3, x_4, … x_n), the associated uncertainty in "S" can be computed employing the error propagation formula delineated in Eq. (6).

$$\frac{\partial S}{S} = \sqrt{\left(\frac{\partial x_1}{x_1}\right)^2 + \left(\frac{\partial x_2}{x_2}\right)^2 + \left(\frac{\partial x_3}{x_3}\right)^2 + \ldots\ldots\ldots\ldots \left(\frac{\partial x_n}{x_n}\right)^2} \tag{6}$$

where, $\frac{\partial x_1}{x_1}, \frac{\partial x_2}{x_2}, \frac{\partial x_3}{x_3}$ etc., denoted the quantified uncertainties attributed to the independent variables, reflecting the propagation of measurement

Table 6
Transesterification acquirements of wasted cooking oil.

Attributes	Sample 1	Sample 2	Sample 3
Freed fatty acid	1.77 %	1.05 %	2.1 %
Catalyst (NaOH) quantity	5 g	5 g	5 g
Oil to Methanol molar ratio	1:6	1:6	1:6
Temperature	~65 °C	~65 °C	~65 °C
Mixing time	90 min	90 min	90 min
output	90.66 %	93.7 %	88.5 %

Table 7
Features of fuel samples.

Properties	ASTM	Diesel	$WCOB_1$	$WCOB_2$	$WCOB_3$	WPO
Density @15 °C in gm/cc	D2709	0.81	0.811	0.792	0.785	0.82
Kinematic Viscosity @40 °C in cst	D445	1.9	2.2	1.65	2.4	1.8
Gross Calorific range in Kcal/kg	D4809–13	9725	8340	9630	7980	7856
Formulated Cetane Index	D976	47	46	56	45	45
Flash indicative by Pensky Martens in ^{O}C	D93	65	104	82	90	112
Conradson Carbon Residue in %	D189	0.02	Nil	Nil	Nil	Nil
Sulfur	D2622	Nil	Nil	Nil	Nil	Nil
Acidity cumulative mg of KOH/g Max	D664	0.1	Nil	Nil	Nil	Nil

inaccuracies inherent in each parameter influencing the overall calculated outcome.

4. Synthesis pathway for bio-derived esters

Biodiesel was produced from waste cooking oil via base-catalyzed transesterification, a process where triglycerides react with methanol in the presence of sodium hydroxide (NaOH) to form fatty acid methyl esters (FAMEs) and glycerol. To maximize FAME yield while reducing unwanted soap formation, the reaction conditions were optimized to a 6:1 methanol-to-oil molar ratio, 1 % NaOH catalyst (by weight), and a temperature of 65 °C, achieving a conversion efficiency exceeding 90 %. The use of excess methanol helped drive the reaction toward higher biodiesel production. Completion of the transesterification process was verified by observing glycerol layer separation and further validated through acid-base titration of the purified biodiesel phase. This ensured minimal residual catalyst and free fatty acids in the final product.

4.1. Catalytic lipid reconfiguration for bio-Ester synthesis

This procedure employs sodium hydroxide briquets (commercially known as caustic soda) as the catalytic agent, though caustic flaking serves as a substitute. A catalyst solution was prepared by dissolving 4.5 g of NaOH in 250 ml of methanol, followed by continuous agitation for 30 min to ensure homogeneity. To avoid agglomeration, the sodium hydroxide pellets were maintained in a moisture-free environment. The methanol-catalyst blend was introduced into the oil contained in a conical flask and subjected to magnetic stirring at 240 rpm for two hours at a controlled temperature of 65 °C. An excess amount of methanol was employed to drive the complete transesterification of triglycerides into methyl esters. Initially, the catalyst preferentially reacts with free fatty acids, initiating saponification. Oils characterized by elevated moisture or free fatty acid concentrations risk emulsion formation, potentially impairing phase separation and overall reaction efficiency unless adequately controlled. A 4.5 g NaOH catalyst was dissolved in 250 mL methanol under constant stirring (240 rpm) using a magnetic stirrer for 30 min at room temperature (~28 °C) to achieve complete dissolution. This methanol-catalyst mixture was then added to preheated waste cooking oil (65 °C) in a conical flask, and the reaction was allowed to proceed for 2 h with continuous stirring under closed conditions to prevent moisture absorption. After completion, the mixture was left undisturbed for 8 h to facilitate phase separation into biodiesel (upper layer) and glycerol (lower layer). The homogeneity and purity of the biodiesel were verified through visual inspection and acid-base titration, confirming successful glycerol removal and high ester content.

4.2. Post-reaction purification and moisture removal of biodiesel esters

Following the separation of glycerol, the resultant methyl esters undergo a purification stage involving multiple warm water rinses to eliminate residual catalysts, soaps, and unreacted contaminants. These esters are then transferred into dedicated storage vessels pending dispatch. A separating funnel was utilized during the post-reaction phase to effectively stratify the ester layer from settled byproducts. Quantitative assessments were carried out to evaluate the proportions of glycerol, coloring agents, and other residual compounds. A washing protocol involving 5 % water (by volume) was employed to ensure the esters reached acceptable cleanliness levels. Subsequently, the biodiesel underwent thermal drying, followed by exposure to ambient airflow via an electric fan for a period of 12 h to remove entrained moisture. The processed biodiesel was then subjected to yield quantification and archived for subsequent physicochemical characterization. In certain cases, when high-quality, low-FFA feedstock is utilized, the water-washing step can be bypassed, yielding esters with purity above 98 %, deemed appropriate for direct fuel applications. For enhanced refinement, vacuum distillation may be employed to further increase ester purity. The intensity of the purification phase is directly influenced by the initial free fatty acid concentration; higher FFA levels necessitate more rigorous post-processing, albeit at the expense of overall biodiesel yield. Table 6 encapsulates the key transesterification conditions used for processing waste cooking oil.

4.3. Thermal depolymerization of LDPE for pyrolytic oil production

Low-density polyethylene (LDPE) was selected as the feedstock for thermal decomposition due to its high availability and substantial role in the plastic waste stream within Chennai, India. The treatment process began with decontamination and mechanical size reduction of LDPE, followed by thermal cracking within an oxygen-restricted reactor chamber operated at temperatures scaling from 450 °C to 750 °C. A resistive copper coil functioned as the primary heat source, initiating polymer breakdown and volatilization. The evolved vapors were directed through a condensation unit maintained at 32 °C using a chilled water-ice system. This facilitated phase transition of volatile organics into a liquid hydrocarbon fraction commonly referred to as pyrolytic oil which accumulated at the condenser's outlet. The entire pyrolytic conversion cycle spanned roughly 90 min, yielding an average of 55 % liquid hydrocarbons by mass, along with secondary products including 30 % waxy residue and approximately 15 % non-condensable gases and solid char. Peak oil yield was observed near 500 °C, indicating it as the optimal cracking temperature for efficient LDPE depolymerization.

4.4. Formulation of waste plastic-derived pyrolysis oil blends and their fuel characteristics

To achieve molecular-level integration of biodiesel/diesel, and wasted plastic oil (WPO), an ultrasonic emulsification protocol was employed. A Hielscher ultrasonicator coupled with a Bioruptor system,

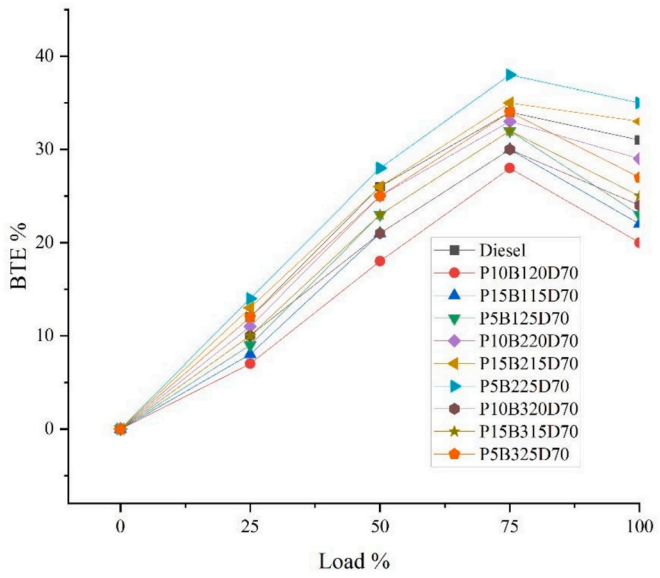

Fig. 3. Brake thermal activity at 200 bar for blends.

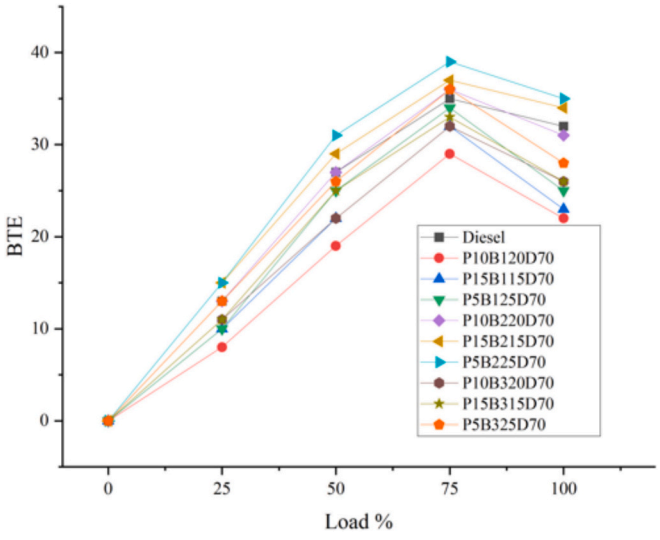

Fig. 4. Brake thermal activity at 230 bar for blends.

operating at 20 kHz within a thermally regulated aqueous bath, enabled the generation of intense acoustic cavitation. This cavitation, transmitted via a sonotrode probe into the sample vials, promoted rapid dispersion and miscibility. The blending process was sustained for 30–45 min to ensure compositional uniformity. Three ternary fuel matrices were synthesized: P10B20D70, P15B15D70, and P5B25D70, representing varied volumetric ratios of WPO, biodiesel, and diesel, respectively. Post-synthesis, physicochemical attributes were quantified in accordance with ASTM protocols, validating their operational viability for compressive ignition drives (Table 7).

To achieve molecular-level integration of biodiesel, diesel, and WPO, an ultrasonic emulsification protocol was used. The blending was conducted using a Hielscher UP400S ultrasonicator operating at 20 kHz and 400 W, combined with a Bioruptor bath held at a constant 35 °C. The sonication process lasted for 30 to 45 min depending on blend composition. Homogeneity was ensured by conducting triplicate stability checks at 1-h intervals, confirming no phase separation or layer stratification. Additionally, optical transparency and droplet dispersion uniformity were visually validated using a laser pointer beam test and low-

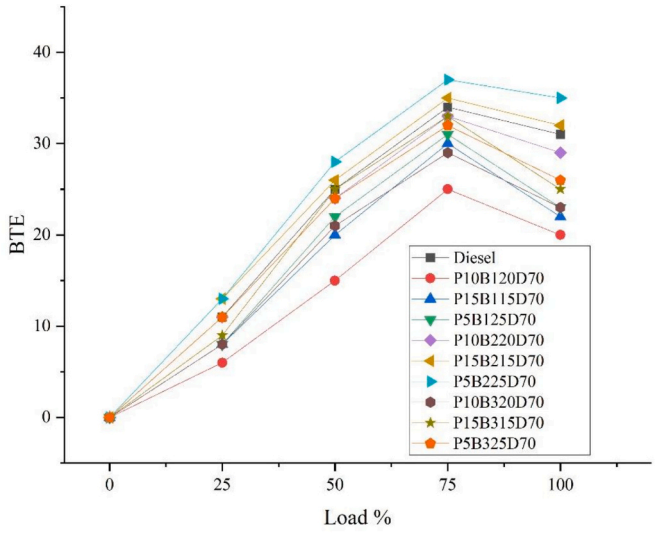

Fig. 5. Brake thermal activity at 170 bar for blends.

speed centrifuge testing (3000 rpm, 10 min), which confirmed blend stability.

5. Quantitative assessment of engine operational metrics and thermodynamic efficiency

Aligned with the experimental design and overarching research goals, an in-depth empirical study was carried out to assess the behavior of ternary fuel systems incorporating waste-derived biodiesel. This chapter delineates the outcomes of that investigation. For benchmarking purposes, both neat diesel (D100) and a standard 20 % biodiesel blend (B20) were evaluated under identical operational conditions. Injection pressure within the compression ignition engine was fine-tuned through direct mechanical alteration of the fuel injection apparatus. The formulated test fuels comprised varying ratios of thermally cracked plastic-derived oil, transesterified biodiesel sourced from three distinct feedstock batches, and conventional diesel. As examples, the nomenclature P10B120D70 denotes a blending of 10 % pyrolytic oil, 20 % biodiesel from batch 1, and 70 % diesel; Concisely, P15B115D70 and P5B125D70 incorporate 15 % and 5 % pyrolytic oil, respectively, with complementary adjustments in biodiesel content from the same batch. This structured formulation strategy was systematically replicated hiring biodiesel derived from batch 2 (P10B220D70, P15B215D70, P5B225D70) and batch 3 (P10B320D70, P15B315D70, P5B325D70). These fuel composites were synthesized and subjected to rigorous evaluation to establish their suitability for CI engine utilization.

5.1. Thermal energy utilization efficiency in engine operation

Brake thermal efficiency (BTE) quantifies the ratio of an engine's useful output power to the thermal energy input derived from the combustion of fuel. This metric is influenced substantially by the fuel's calorific value and mass density, both of which dictate the energy conversion potential. Figs. 3, 4, and 5 illustrate the trends in BTE across varying engine loads for a suite of ternary fuel combinations—ranging from baseline diesel (D100) to formulations like P10B120D70, P15B115D70, P5B125D70, P10B220D70, P15B215D70, P5B225D70, P10B320D70, P15B315D70, and P5B325D70. These experiments were conducted under three distinct fuel injection pressures, enabling a comparative assessment of how injection pressure modulations affect thermal conversion performance across all tested blends.

The experimental results demonstrate a nuanced relationship between fuel type and brake thermal efficiency (BTE). While neat diesel maintains superior average BTE (19.69 %) across all test conditions due

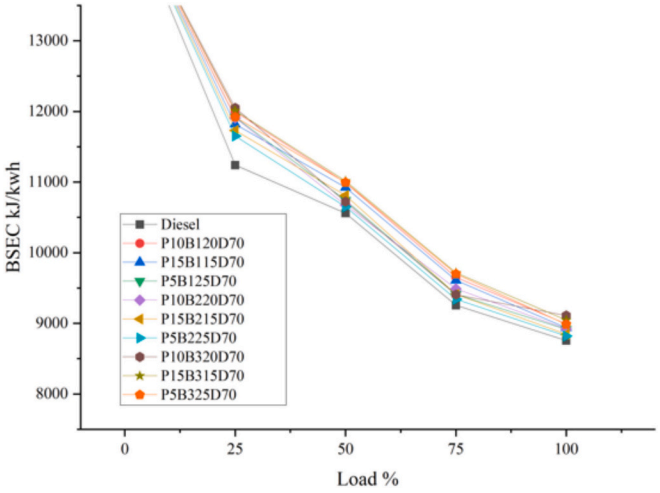

Fig. 6. BSEC of several blends at 200 bar.

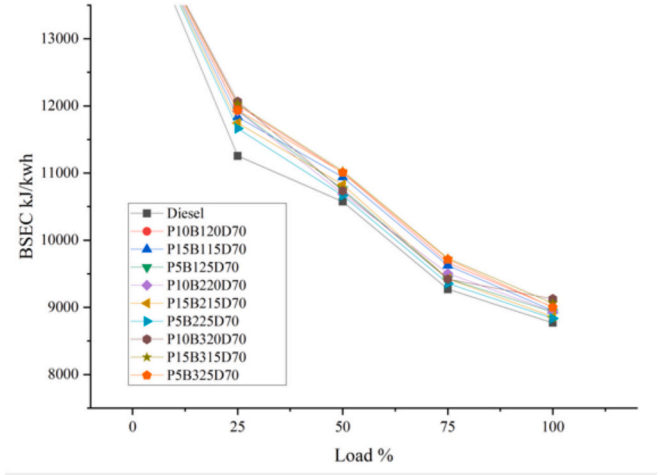

Fig. 7. BSEC of several mixes at 230 bar.

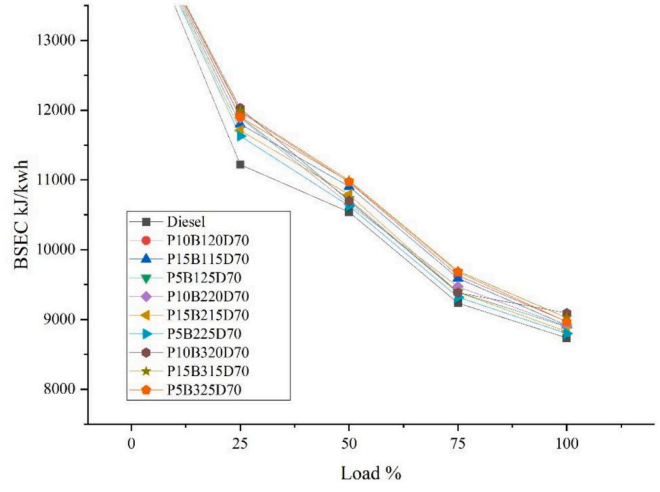

Fig. 8. BSEC of several mixes at 170 bar.

to its higher energy density, detailed analysis reveals that optimized ternary blends can achieve comparable performance under specific operating parameters. Most notably, the P10B220D70 blend reaches

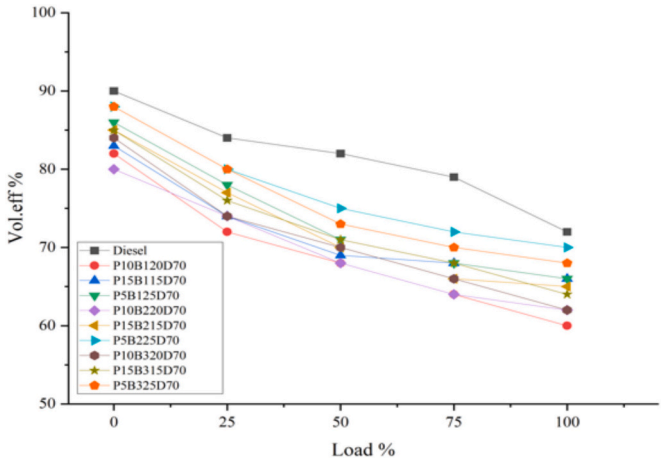

Fig. 9. Volumetric efficacy of several mixes at 200 bar.

19.65 % BTE at 230 bar injection pressure, nearly matching diesel's maximum efficiency, as evidenced in Figs. 3–5. This exceptional performance stems from the combined effects of enhanced spray atomization and the oxygenated nature of the biodiesel component, which promotes more complete combustion at elevated injection pressures. However, this parity is pressure-dependent - at conventional 200 bar injection pressure, the same blend shows 0.5–1.5 % lower efficiency than diesel, while at 170 bar, the performance gap widens to 2–3 % due to compromised atomization quality. Diesel's efficiency remains remarkably stable across pressure variations (ΔBTE <0.5 %), whereas the ternary blends exhibit greater sensitivity to injection parameters. All fuel configurations follow characteristic load-efficiency curves, with peak performance typically occurring between 75 and 100 % load. These findings collectively demonstrate that while diesel maintains an overall efficiency advantage, proper calibration of injection pressure can enable carefully formulated waste-derived blends to achieve diesel-competitive thermal efficiency in optimized operating conditions. The P10B220D70 blend achieves a brake thermal efficiency (BTE) of 19.65 % at an injection pressure of 230 bar, closely approaching conventional diesel's 19.69 % BTE. This result supports the findings of Sowmiya et al. [32], who reported enhanced thermal efficiency for waste cooking oil (WCO) biodiesel blends under higher injection pressures.

5.2. Quantitative assessment of brake specific energy consumption

Brake specific energy consumption (BSEC) serves as a metric for assessing the energy demand of a fuel to generate one kilowatt-hour of mechanical output, thus providing a direct indication of combustion effectiveness and fuel economy.

This parameter is strongly governed by the intrinsic energy density and mass characteristics of the fuel. Figs. 6 through 8 present the BSEC profiles corresponding to neat diesel and multiple ternary fuel combinations, evaluated across three injection pressures. Due to reduced heat content, biodiesel-based mixtures generally exhibit elevated BSEC values compared to diesel. The average BSEC determined for 100 % diesel was approximately 9545.7 kJ/kW-h, whilst blends incorporating biodiesel from sample 1, sample 2, and sample 3 recorded mean values of 10,565, 10090, and 10,625 kJ/kW-h, respectively. Among these, blends derived from sample 2 consistently displayed the most favorable (i.e., lowest) energy consumption rates. At a standard injection setting of 200 bar, diesel recorded a BSEC of 9755 kJ/kW-h. In contrast, the biodiesel mixes ranged between 9785 and 10,515 kJ/kW-h hinging on injective load variation. Notably, increasing the injection pressure enhanced combustion efficiency for biodiesel fuels, yielding lower BSEC outcomes.

Across all operative loadings, the specific energy consumption for

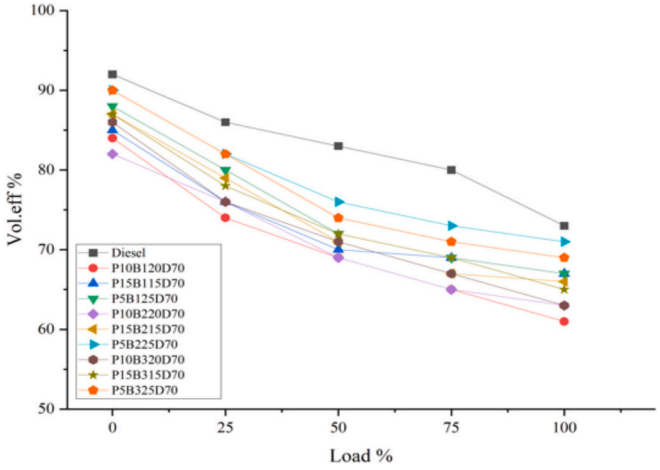

Fig. 10. Volumetric efficacy of several mixes at 230 bar.

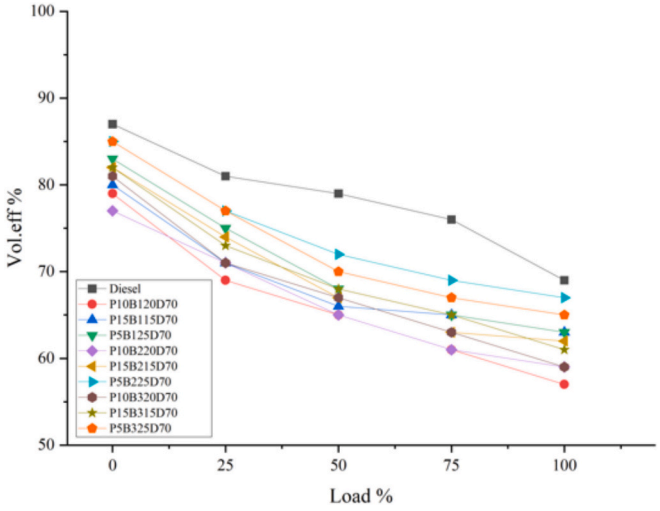

Fig. 11. Volumetric efficacy of several mixes at 170 bar.

sample 1 blends—P10B120D70, P15B115D70, and P5B125D70—averaged 10,410 kJ/kW-h, 10,210 kJ/kW-h, and 10,810 kJ/kW-h, respectively, corresponding to standard, elevated, and reduced injection pressures. Similarly, sample 3 blends—P10B320D70, P15B315D70, and P5B325D70—demonstrated specified energy consumptions of 9985 kJ/kW-h, 9915 kJ/kW-h, and 10,530 kJ/kW-h across all load conditions. Elevated injection pressures induced earlier combustion timing, bringing peak cylinder pressures nearer to the Top Dead Center (TDC). In contrast, lowering injection pressure to 170 bar resulted in a delayed peak pressure occurrence. Notably, at higher injection pressures, the BSEC trends of all fuel blends closely mirrored those of neat diesel. Increasing engine load generally reduced the energy required per unit power for every fuel combination. At elevated loads, the specific energy consumption values converged across blends and injection pressures, while at lighter loads, diesel usage remained consistently lower regardless of injection pressure settings.

5.3. Aspirated volume efficiency assessment

Figs. 9, 10, and 11 present the volumetric efficacy outcomes for the blends P10B120D70, P15B115D70, P5B125D70, P10B220D70, P15B215D70, P5B225D70, P10B320D70, P15B315D70, and P5B325D70 under three distinct injection pressure settings. Volumetric efficiency is a vital parameter in air-breathing engines, warranting

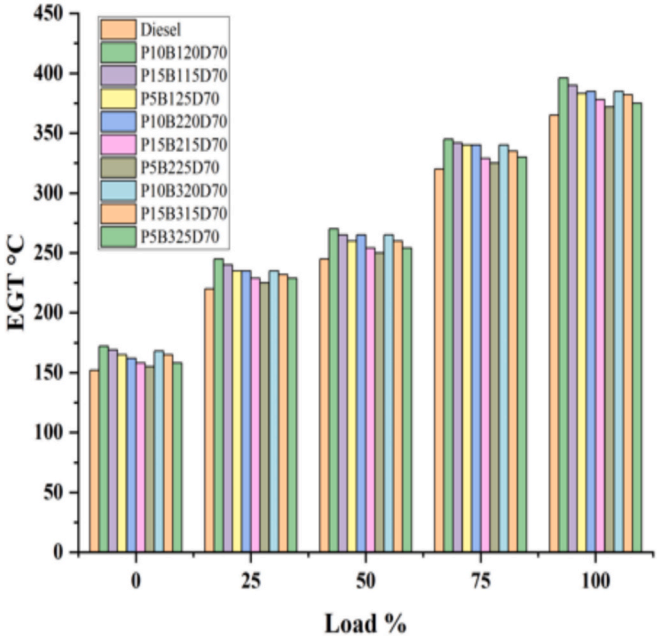

Fig. 12. Exhaustive vapor Temp of several mixes at 170 Bar.

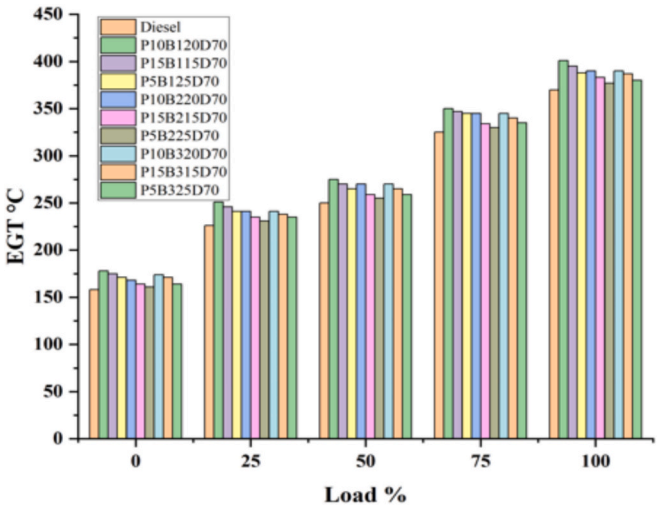

Fig. 13. Exhaustive vapor Temp of several mixes at 200 Bar.

thorough examination due to its direct influence on engine performance. This efficiency is affected by both the engine's operational conditions and ambient environmental factors.

Across varying engine loading and injective loads, purer diesel consistently demonstrates superior averaged volumetric efficacy, measured at 82.46 %, largely due to its higher calorific content. In contrast, biodiesel mixes derived from samplings 1, 2, and 3 exhibit lower averaged efficiencies of 79.65 %, 76.92 %, and 78.25 %, respectively. At the standardized injective load of 200 bar, diesel achieves a volumetric efficiency of 80.95 %, which rises to 83.12 % at 230 bar and declines to 78.9 % when the pressure drops to 170 bar. Correspondingly, sample 2 blends record volumetric efficiencies of 80 %, 80.15 %, and 76.3 %, while sample 1 blends show 76.55 %, 78.88 %, and 76.95 %, and sample 3 blends achieve 78.15 %, 78.95 %, and 77.25 % at the same pressures. The data reveal a clear trend: elevated injection pressures enhance volumetric efficiency, whereas lower pressures diminish it, independent of load conditions. Although differences between diesel and biodiesel blends are marginal under light loads, the disparity widens

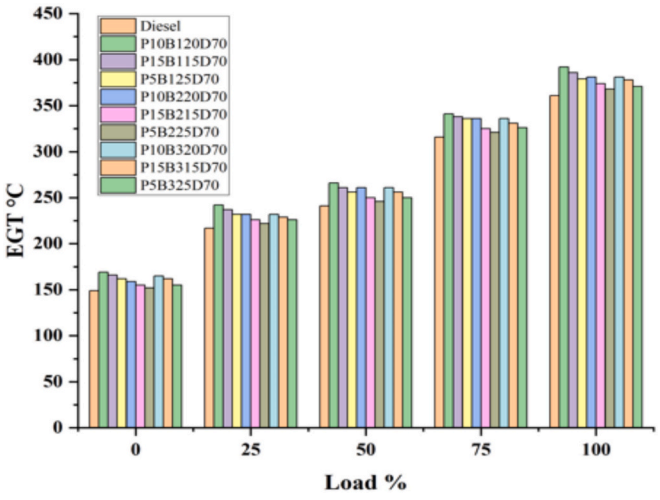

Fig. 14. Exhaustive vapor Temp of several mixes at 230 Bar.

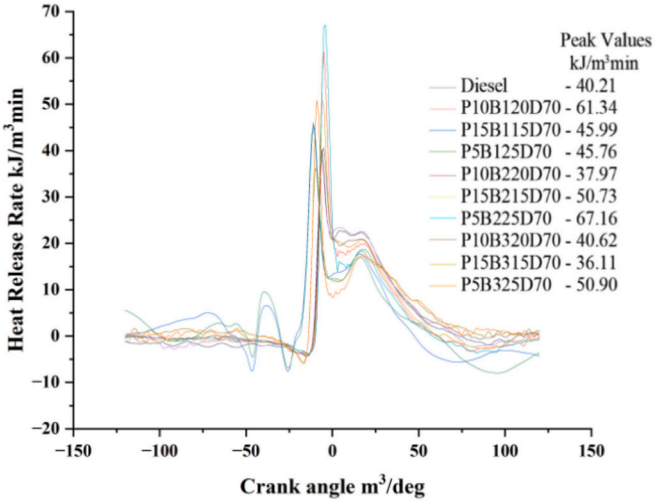

Fig. 17. 200 bar Full-loading HRR of several mixes.

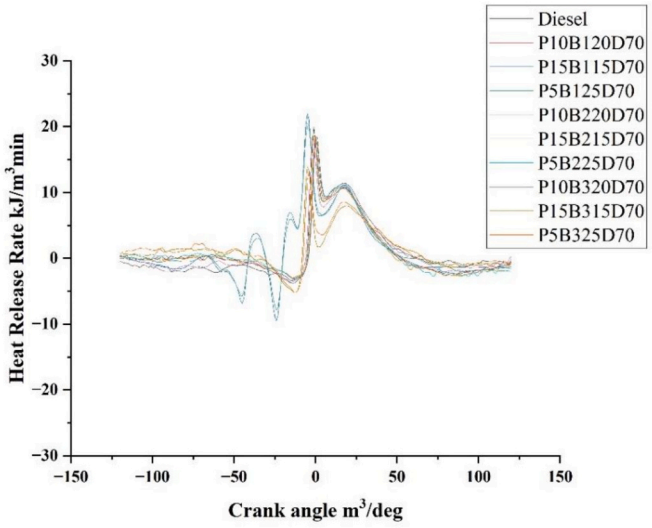

Fig. 15. 200 bar zero-loading HRR of various mixes.

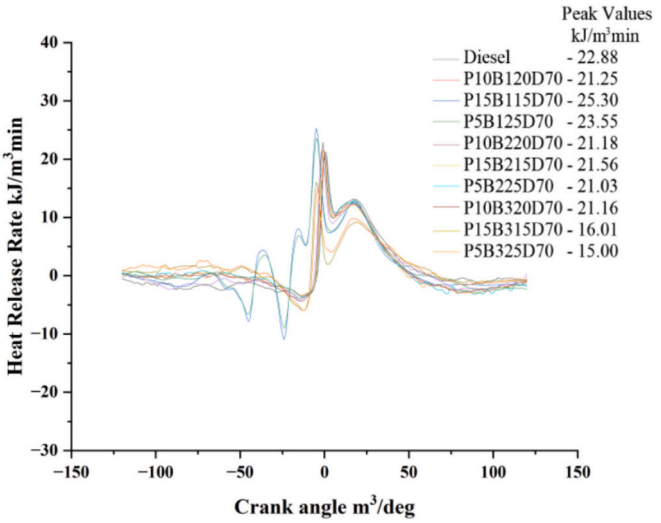

Fig. 18. 230 bar Zero-loading HRR of several mixes.

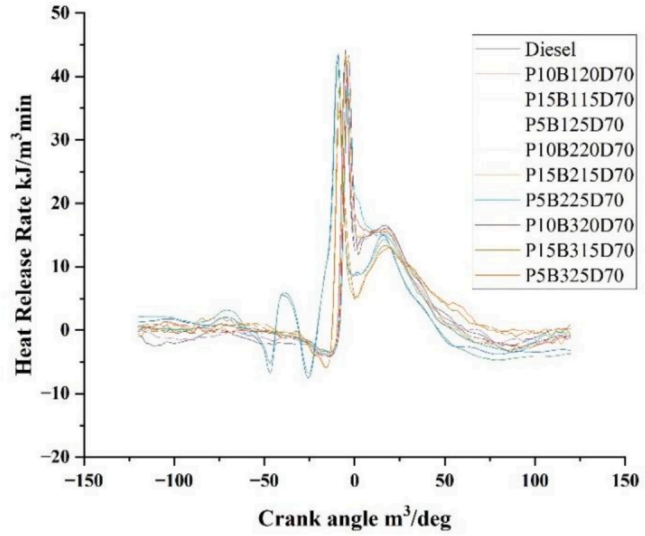

Fig. 16. 200 bar Half-loading HRR of several mixes.

considerably at full load, with biodiesel blends exhibiting a marked drop in volumetric efficiency. This reduction is attributed to incomplete combustion and diminished air intake, stemming from increased exhaust back pressure under heavy engine operation.

5.4. Combustion exhaust thermal profile

The exhaust gas temperature emitted by the engine serves as an important indicator to assess the heat energy utilization during combustion. Figs. 12–14 illustrate the exhaustive heating scalings for purer diesel and various fuel mixes including P10B120D70, P15B115D70, P5B125D70, P10B220D70, P15B215D70, P5B225D70, P10B320D70, P15B315D70, and P5B325D70. These measurements were recorded at three distinct injection pressure settings to evaluate their impact on thermal characteristics.

Considering all engine loading and injective pressure variations, the mean exhaustive vapor temperature (EGT) for neat diesel is approximately 256 °C. In disparity, biodiesel blends exhibit elevated average EGTs: 278 °C for sample 1, 269 °C for sample 2, and 282 °C for sample 3, implying comparatively reduced thermal efficiency. Among these, sample 2 demonstrates the lowest exhaust temperature, indicating more effective combustion performance. For diesel, EGT values average

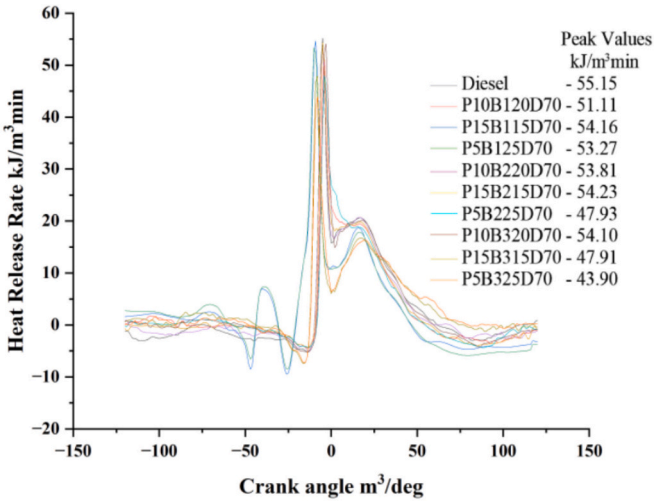

Fig. 19. 230 bar Half-loading HRR of several mixes.

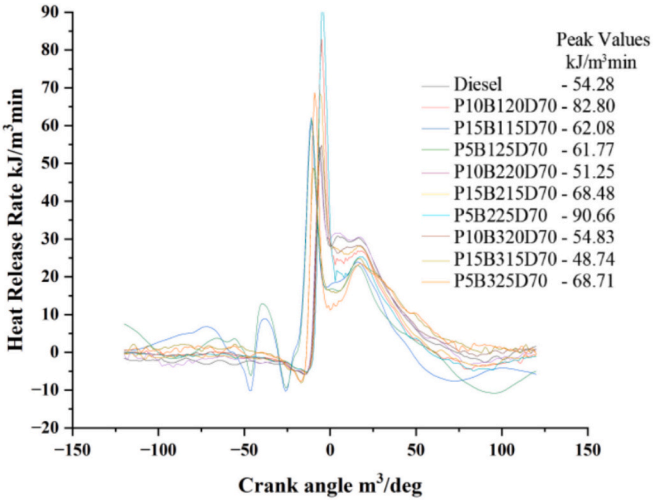

Fig. 20. 230 bar Full-loading HRR of several mixes.

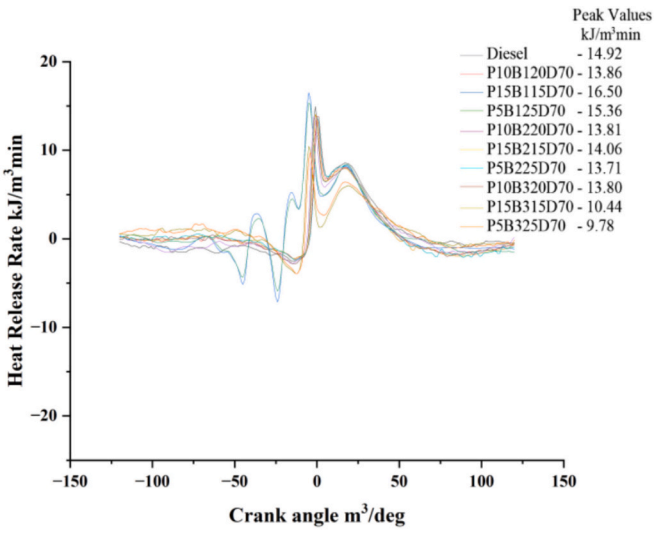

Fig. 21. 170 bar Zero-loading HRR of several mixes.

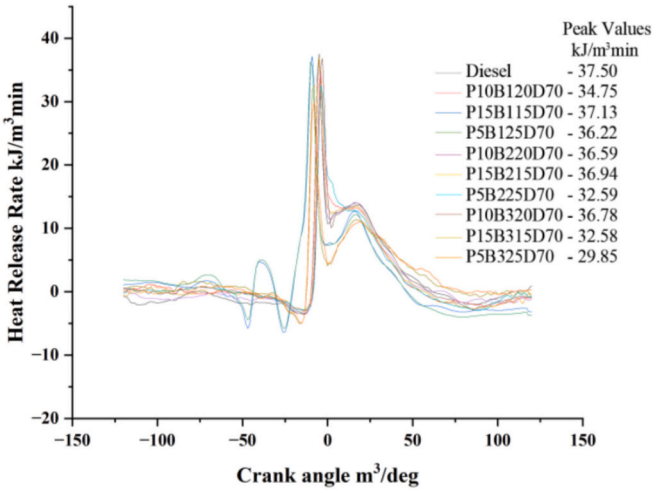

Fig. 22. 170 bar Half-loading HRR of several mixes.

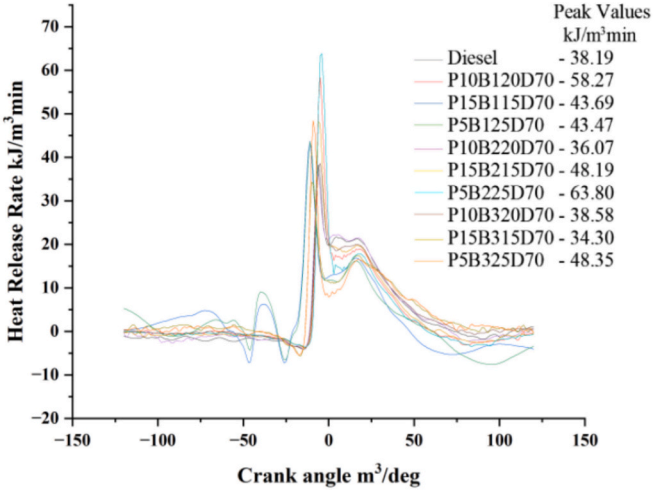

Fig. 23. 170 bar Full-loading HRR of several mixes.

261 °C at 200 bar, increase to 285 °C at 230 bar, and decrease to 250 °C at 170 bar. Corresponding temperatures for sample 2 blends are 273 °C, 298 °C, and 260 °C, respectively. Sampling 1 mixes register 280.45 °C, 310 °C, and 278 °C, while sample 3 records 281.55 °C, 306 °C, and 269 °C at the same pressure levels. Elevated injection pressures correlate with increased EGT due to higher combustion chamber temperatures and intensified heat transfer. The rise in exhaust gas temperature (EGT) at elevated injection pressures follows the pattern reported by Jene et al. [33], who linked this phenomenon to improved heat release characteristics during combustion. Moreover, EGT consistently rises with engine load across all fuels, reaching peak values under maximum load conditions, reflecting intensified combustion activity and thermal stress.

6. THERMO-combustive behavior analysis

6.1. Heat evolution dynamics during combustion

The heat release extreme (HRR) quantifies the thermal energy generated during the combustion of fuel within the engine cylinder, which elevates the internal acquisition of the working sample and is subsequently transformed into mechanised output. A fraction of this thermal energy dissipates through the cylinder walls, cylinder head, and engine cooling mechanisms. Figs. 15 through 23 illustrate the temporal variation of HRR as a function of crank angle for pure diesel and multiple

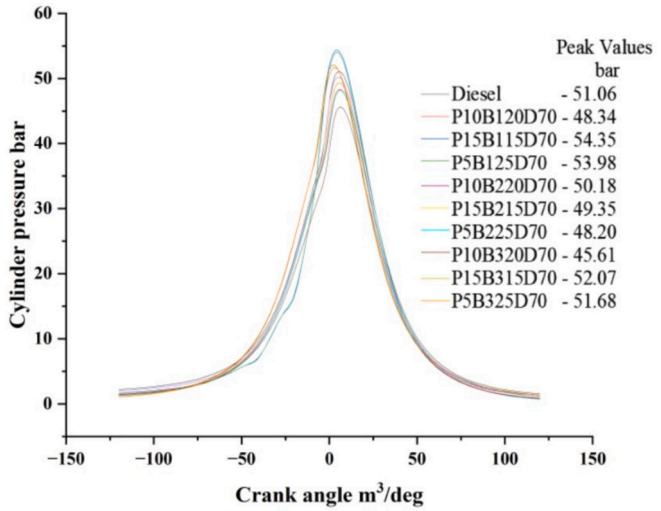

Fig. 24. Cylinder loading at 200 bar for Zero rate.

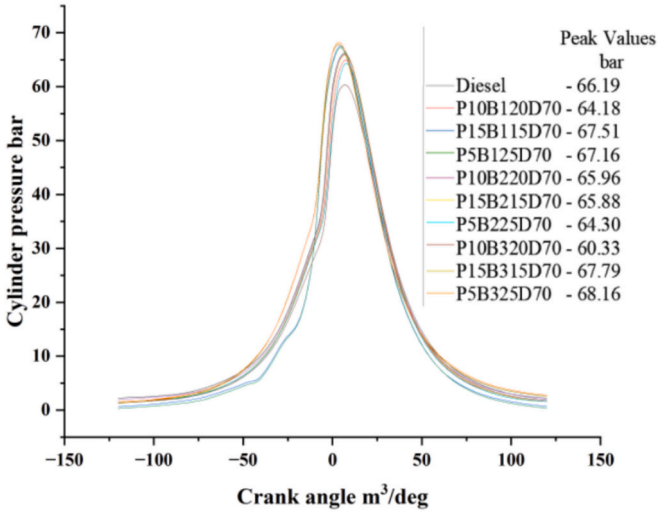

Fig. 25. Cylinder loading at 200 bar for Half bearing.

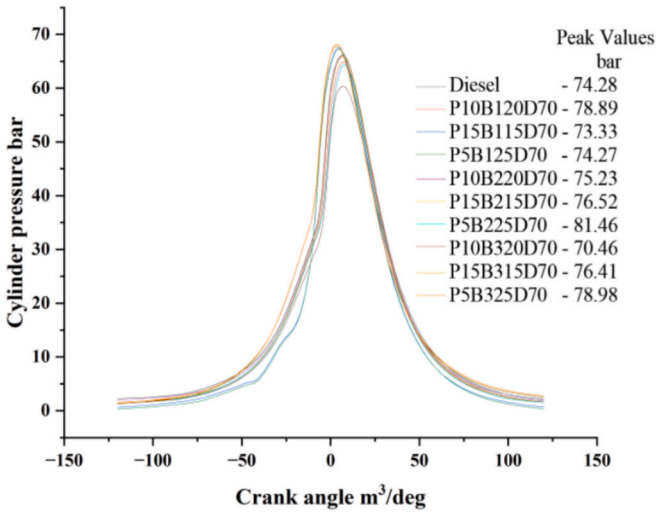

Fig. 26. Cylinder loading at 200 bar for Full bearing.

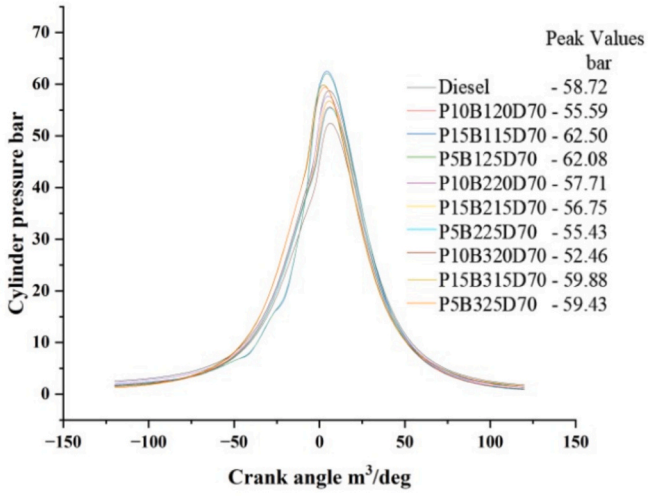

Fig. 27. Cylinder loading at 230 bar for Zero rating.

biodiesel blends (including P10B120D70, P15B115D70, etc.) under varying injective pressures and load conditions. Both diesel/biodiesel mixes display a characteristic two-stage combustion phenomenon: an initial rapid intermixed combustion phase pre-cursored by a slower diffusion-controlled combustion phase. Post ignition delay, the pre-mixed fuel-air mixture undergoes swift combustion, resulting in a pronounced spike in heat release, which then transitions into the prolonged diffusion combustion stage. Notably, biodiesel blends tend to exhibit accelerated premixed combustion compared to neat diesel. Averaged over all operational parameters, diesel's HRR stands at approximately 63.65 kJ/m^3.°CA, whereas biodiesel mixes derived from sampling 1, 2, and 3 present slightly elevated values of 65.25, 63.54, and 66.55 kJ/m^3.°CA respectively, indicating subtle variations in combustion dynamics attributable to fuel composition.

At an injection pressure of 200 bar, the mean heat release rate (HRR) for pure diesel registers at 64.88 kJ/m^3.°CA across various engine loads. Increasing the injection pressure to 230 bar elevates the HRR to 70.77 kJ/m^3.°CA, whereas reducing the pressure to 170 bar lowers it to 54.23 kJ/m^3.°CA. Biodiesel mixes from sampling 2 demonstrate HRR scaling of 63.45, 70.53, and 55.10 kJ/m^3.°CA at 200, 230, and 170 bar, respectively. Similarly, sampling 1 mix exhibit HRRs of 68.32, 74.55, and 56.24 kJ/m^3.°CA across the same pressure spectrum. The median heat release rates for the three blend categories at 200, 230, and 170 bar are observed to be 70.5, 74.65, and 57.65 kJ/m^3.°CA, respectively. Notably, the HRR tends to decline at elevated injection pressures near 230 bar but shows a marked increase when operating below 170 bar. Under full load conditions at 170 bar, pure diesel attains its peak HRR value of 88.8 kJ/m^3°CA. Correspondingly, maximum HRRs for the biodiesel blends span from 86.29 to 88.57 kJ/m^3°CA. The biodiesel blends exhibited faster premixed combustion, consistent with findings reported by Sufe et al. [34] for comparable ternary fuel systems. This progressive rise in heat release rate with increased engine load correlates directly with augmented combustion chamber temperatures and pressures, intensifying the combustion process.

6.2. *Pressure behavior inside cylinder*

Figs. 24 illustrate the variation of in-cylinder pressure as a function of crank angle for pure diesel and various biodiesel blends (e.g., P10B120D70, P15B115D70) under multiple injection pressures and load scenarios. The transformation of the chemical acquisit contained in the fuel into cylinder loading plays a critical role in defining engine output characteristics and emission profiles. Across all operational conditions, pure diesel exhibited an average cylinder pressure of 65.6 bar. In juxtaposition, biodiesel mix from sampling 1, 2, and 3 recorded mean

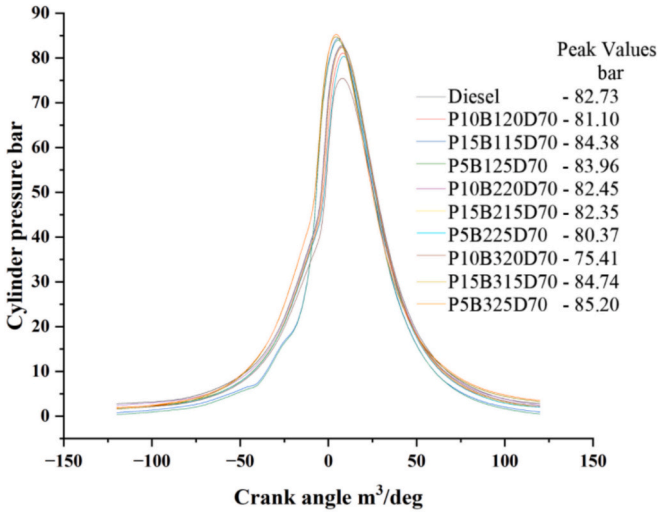

Fig. 28. Cylinder loading at 230 bar for Half bearing.

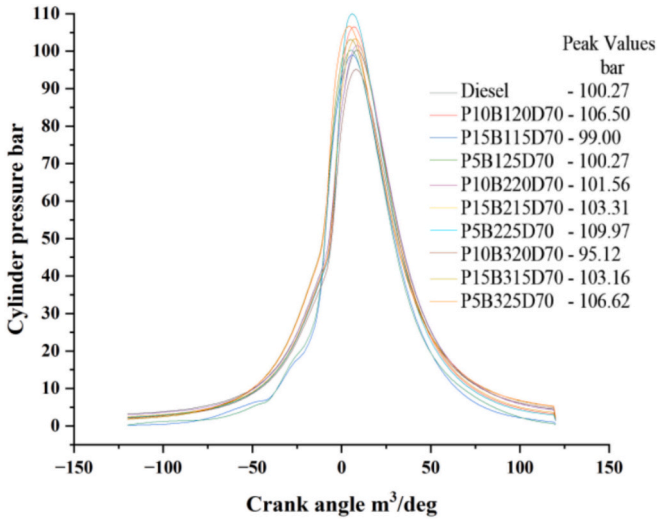

Fig. 29. Cylinder loading at 230 bar for Full bearing.

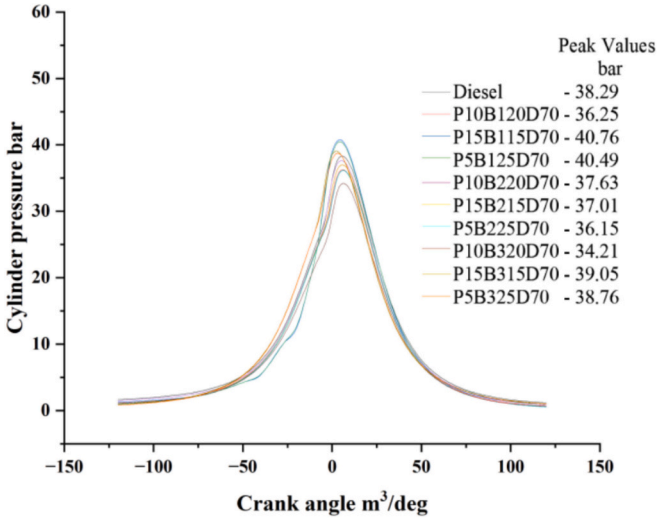

Fig. 30. Cylinder loading at 170 bar for Zero rating.

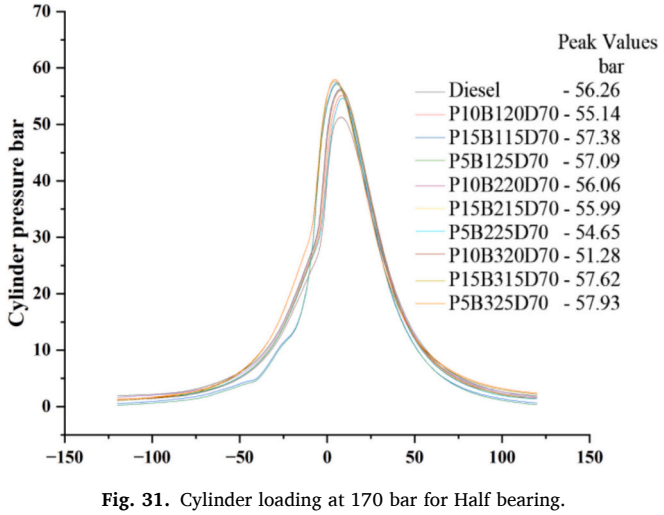

Fig. 31. Cylinder loading at 170 bar for Half bearing.

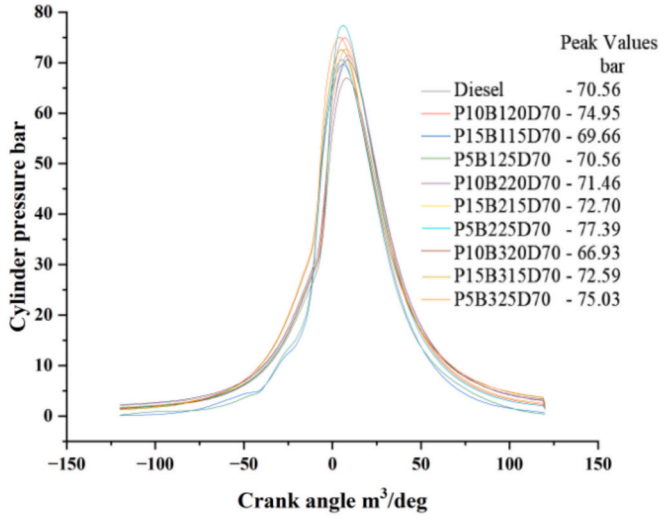

Fig. 32. Cylinder loading at 170 bar for Full bearing.

pressures of 61.88 bar, 63.9 bar, and 60.55 bar, respectively. At an injective loading of 230 bar under full load, pure diesel approximated a maximum cylinder loading of 72.5 bar. Similarly, biodiesel blends attained peak pressures at full load with values of 72.5 bar for P5B225D70, 69.85 bar for P5B125D70, and 68.5 bar for P15B315D70. Generally, peaked cylinder loading was most pronounced at the highest injectable loading level of 230 bar. The comparatively lower peak pressures observed in biodiesel blends are primarily associated with reduced ignition delay periods and diminished diffusion combustion efficiency. Among the mix, sampling 2 demonstrated superior peaking pressure performance, a phenomenon attributable to its comparatively lower viscosity and enhanced calorific content, facilitating more thorough combustion within the cylinder. (See Figs. 25–32.)

At the baseline injectable loading of 200 bar, neat diesel exhibits an average in-cylinder pressure of approximately 65.65 bar over varying load conditions. This value rises notably to 81.45 bar when the injection pressure is elevated to 230 bar, while at a reduced pressure of 170 bar, the pressure remains near 65.65 bar. Biodiesel mix from sampling 2 shows cylinder pressure scaling of 63.0, 66.85, and 62 bar at injection pressures of 200, 230, and 170 bar, respectively. Correspondingly, sampling 1 mixes measure 64, 66.5, and 58.5 bar, whereas sampling 3 mixes yield 61.8, 64.5, and 60.2 bar across the same loading levels. For all fuel types, the apex of cylinder pressure occurs consistently at the highest injection pressure setting of 230 bar. Augmenting the injection

Table 8
Comparison of Emissions with BS-VI Standards.

Emission Parameter	BS-VI Limit (g/kWh)	Best Observed Blend (at 230 bar)	Measured Value (g/kWh)
NOx	0.4	P5B225D70	0.42
CO	0.5	P10B220D70	0.08
HC	0.1	P15B215D70	0.09
Smoke Opacity	≤ 25 % HSU	P5B225D70	18.5 %

Table 9
Correlation stamping between associatives.

Output Parameter	Fuel Blend Type (A)	*p*-value (A)	Injection Pressure (B)	p-value (B)	Engine Load (C)	p-value (C)
BTE	−0.022	0.738	0.894	0.002	0.048	0.621
VOL EFF	−0.052	0.616	−0.978	0.000	0.059	0.593
Pressure	−0.195	0.198	0.882	0.003	0.243	0.128
CO	−0.278	0.079	−0.071	0.781	−0.034	0.854
HC	0.136	0.374	0.801	0.005	0.086	0.715
Smoke	0.031	0.866	0.869	0.004	−0.161	0.308
NOx	0.071	0.729	0.923	0.001	0.218	0.187
BSEC	0.061	0.765	0.739	0.006	0.027	0.884
EGT	0.122	0.417	0.953	0.000	−0.169	0.281

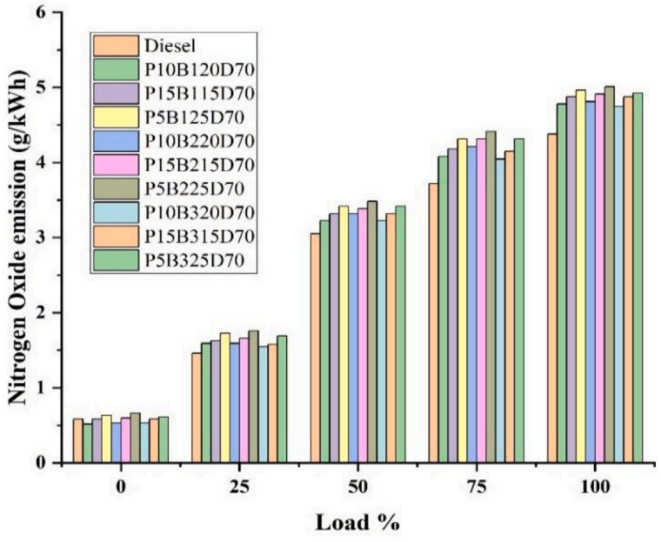

Fig. 33. Nitrogen oxides of several mixes at 200 bar.

pressure leads to an increase in the temperature and density of the intake charge, which subsequently enhances the in-cylinder pressure during combustion. Conversely, lowering the injection pressure tends to postpone the onset of combustion, resulting in diminished combustion efficiency and reduced peak pressure values. Nonetheless, at extreme injection pressures—both low (170 bar) and high (230 bar)—improvements in fuel spray penetration can alter atomization characteristics and combustion dynamics, occasionally causing a decline in peak pressure. Peak cylinder pressures are most prominent under full load conditions, attributable to reduced ignition delay intervals and elevated combustion temperatures. These findings support the potential use of B20 biodiesel blends containing up to 10 % pyrolysis oil as suitable alternative fuels for compression ignition engines [35].

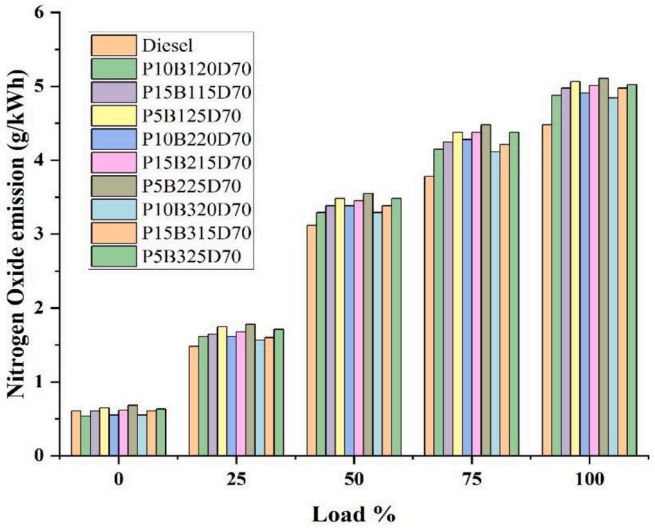

Fig. 34. Nitrogen oxides of several mixes at 230 bar.

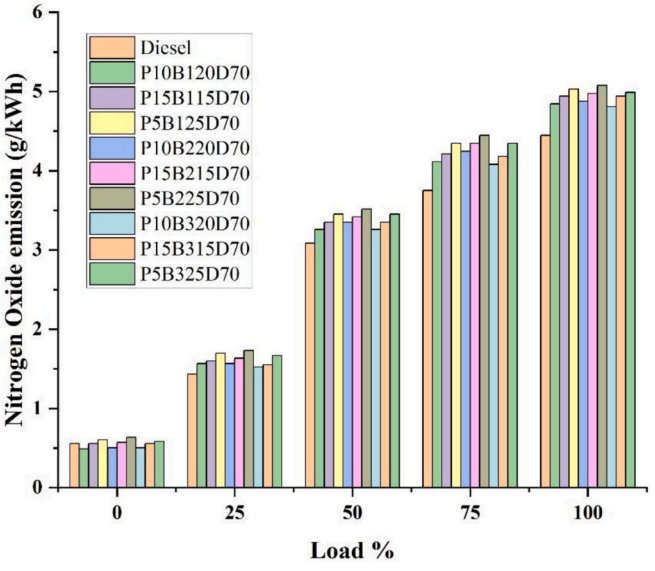

Fig. 35. Nitrogen oxides of several mixes at 170 bar.

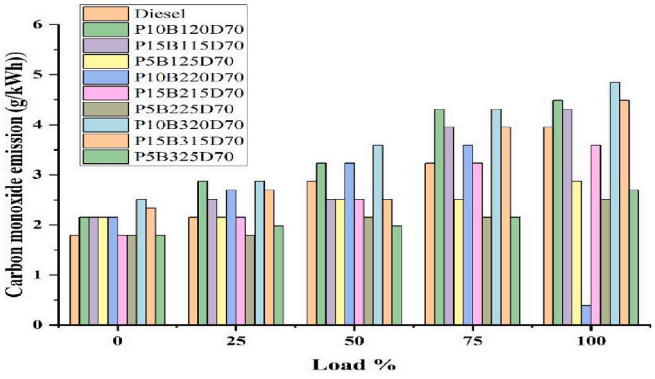

Fig. 36. Carbon monoxide exhaust of involved blends at 200 bar.

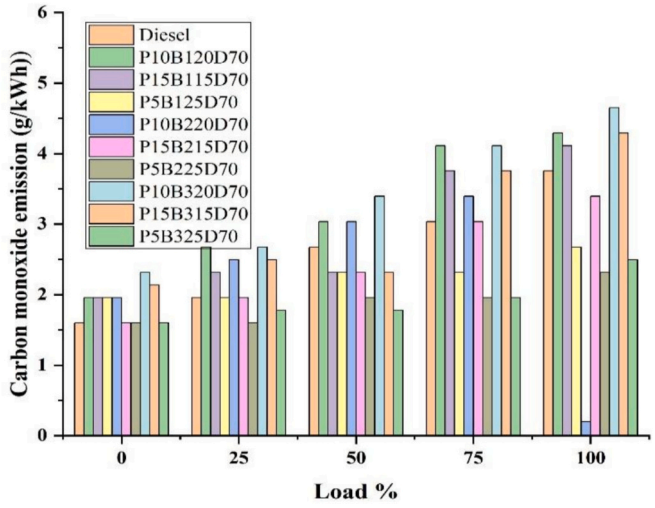

Fig. 37. Carbon monoxide exhaust of involved mixes at 230 bar.

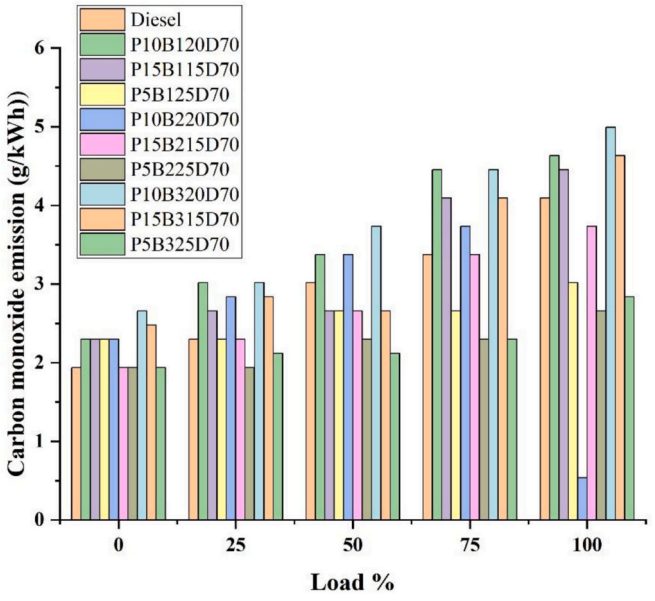

Fig. 38. Carbon monoxide exhaust of involved mixes at 170 bar.

7. Pollutant emission dynamics

7.1. Formation and trends of nitrogen oxides (NOx)

Nitrogenised oxides (NOx) are generated primarily through non conditioned chemical interactions betwixt atmospheric nitrogen and oxygen under high-temperature combustion conditions. In compression ignition engines, the predominant factors driving NOx formation are elevated flame temperatures combined with extended combustion phases. Biodiesel mixes typically contain elevated intrinsic oxygen levels juxtaposed to conventional diesel, which often leads to augmented NOx production. Figs. 33 through 35 illustrate the variation of NOx emissions (measured in ppm) against engine load for neat diesel and multiple biodiesel blends (such as P10B120D70, P15B115D70, P5B125D70, among others) evaluated at three distinct injection pressures. The overall average NOx concentration observed for pure diesel across all operating points and injection settings is 318 ppm. In contrast, biodiesel blends present increased NOx outputs, with mean values of 364 ppm, 410 ppm, and 360 ppm for samples 1, 2, and 3, respectively. Notably, blends like P15B115D70 and P15B215D70 consistently yield the highest NOx emissions, attributable to intensified combustion temperatures and longer residence times in the high-temperature zone. Conversely, blends such as P5B125D70 and P5B225D70 exhibit comparatively lower NOx concentrations, likely due to a moderated rate of premixed combustion which limits peak temperature spikes.

At a baseline injection pressure of 200 bar, diesel fuel exhibits an average NOx concentration of approximately 360 ppm across varying engine loads. This value escalates to around 380 ppm at an elevated injectable loading of 200 bar, while it diminishes to about 220 ppm when the injection pressure is lowered to 170 bar. For the biodiesel blends categorized as sample 2, measured NOx levels are 392 ppm, 462 ppm, and 232 ppm at 200, 230, and 170 bar respectively. Sampling 1 mixes show higher emission values of 428 ppm, 476 ppm, and 327 ppm under the same pressure conditions, whereas sample 3 averages 373 ppm, 458 ppm, and 253 ppm correspondingly. The increase in injection pressure to 230 bar advances the onset of combustion timing, initiating fuel burn prior to the piston reaching top dead center. This shift leads to elevated peak in-cylinder temperatures, which subsequently enhances NOx formation.

Conversely, reduced injection pressures delay the combustion process into the expansion stroke, thereby suppressing peak thermal levels and lowering NOx output. Additionally, NOx emissions demonstrate a clear positive correlation with engine load, as intensified combustion temperatures at higher loads drive increased nitrogen oxide generation. At minimal load conditions, the combustion temperature remains comparatively lower, resulting in reduced NOx formation relative to full-load scenarios where thermal stresses peak. The observed increase in NOx emissions at 230 bar aligns with established thermal NOx formation mechanisms, as documented by Gopal et al. [36]

7.2. Carbon monoxide emission dynamics

Incomplete combustion of hydrocarbon fuels in diesel engines provocates to the expedition of carbon monoxide (CO). Under conditions of sufficient oxygen availability, elevated temperature, and adequate residence time, CO undergoes further oxidation to form carbon dioxide (CO_2). When these conditions are not met, incomplete oxidation results in increased CO emissions. Figs. 36 to 38 depict CO emission levels (signified as percentage) plotted against engine loading for distinguished fuel mixes at three different injectable pressures. Pure diesel exhibits an average CO emission of approximately 0.08 %. Biodiesel mixes from samplings 1, 2, and 3 demonstrate arithmetic emissions of 0.086 %, 0.076 %, and 0.15 %, respectively. Generally, the higher oxygen content in biodiesel blends enhances oxidation reactions, leading to lower CO emissions. However, blends containing higher proportions of pyrolysis oil—such as P15B115D70, P15B215D70, and P15B315D70 show elevated CO emissions at low engine loads, which is attributed to reduced spray quality caused by the elevated viscosity of pyrolysis sample. In juxtapose, blends with lower pyrolysis oil content namely P5B125D70, P5B225D70, and P5B325D70 achieve reduced CO emissions due to improved atomization and more efficient combustion.

At the baseline injectable pressure of 200 bar, diesel fuel exhibits an average carbon monoxide (CO) emission of approximately 0.085 % across varying engine loads and operating ambiences. When the injection pressure is elevated to 230 bar, the mediated CO emission for diesel slightly decreases to 0.007 %, whereas it rises to about 0.08 % at the reduced pressure of 170 bar. For biodiesel blend sample 2, the average CO emissions recorded are 0.066 %, 0.06 %, and 0.072 % at injectable loadings of 200, 230, and 170 bar, respectively, measured over cumulative load ambiences and test cycles. Similarly, sample 1 biodiesel blends show average CO values of 0.07 %, 0.065 %, and 0.073 % at the corresponding injection pressures. Sample 3 blends demonstrate higher CO emissions, averaging 0.138 %, 0.12 %, and 0.15 % at 200, 230, and 170 bar respectively, beyond the entire load spectrum evaluated. The results indicate that elevating injection pressure generally facilitates

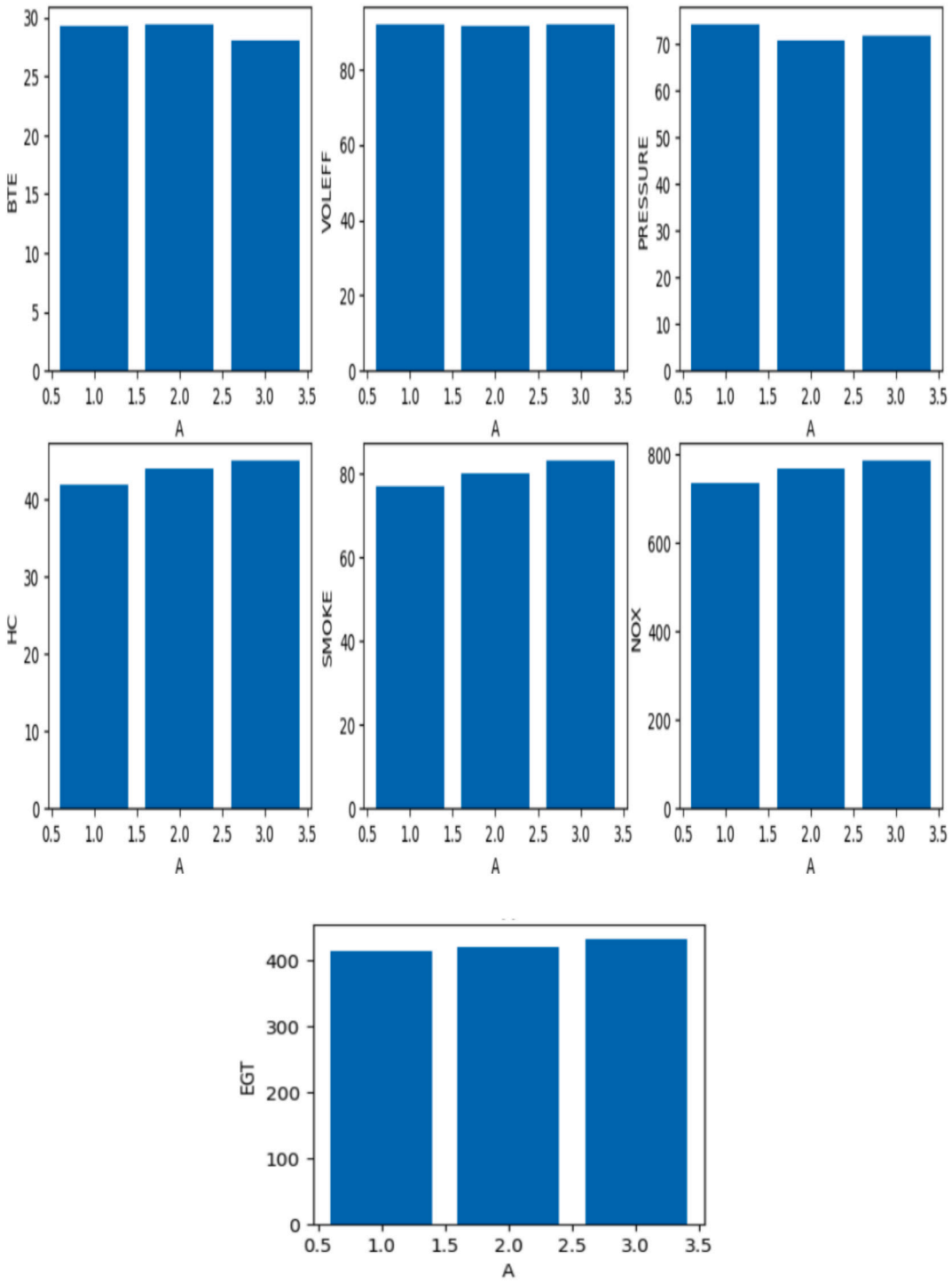

Fig. 39. Illustrates the relationship between A and other associated variables.

more thorough and efficient combustion, thereby marginally reducing CO emissions overall. Conversely, lower injection pressures are associated with increased CO levels, likely due to less effective fuel atomization and incomplete oxidation. Furthermore, CO emissions tend to rise with increasing engine load, although this effect is relatively minor at lower load settings and transient operating conditions. The emission performance of the ternary blends was assessed against Bharat Stage VI (BS-VI) standards for light-duty compression ignition engines. Results demonstrate that CO and HC emissions from all tested blends comply with regulatory limits under full-load operation at 230 bar injection pressure. While blends P5B225D70 and P10B220D70 exhibited NOx emissions slightly exceeding BS-VI thresholds at 200 bar, these levels decreased substantially when injection pressure was reduced to 170 bar. All blends maintained smoke opacity below the 25 % HSU benchmark, confirming efficient combustion. This evidence indicates that waste-derived fuels can achieve compliance with contemporary emission regulations through appropriate injection pressure optimization. Table 8 demonstrates that CO emissions were 25 % below BS-VI limits [37].

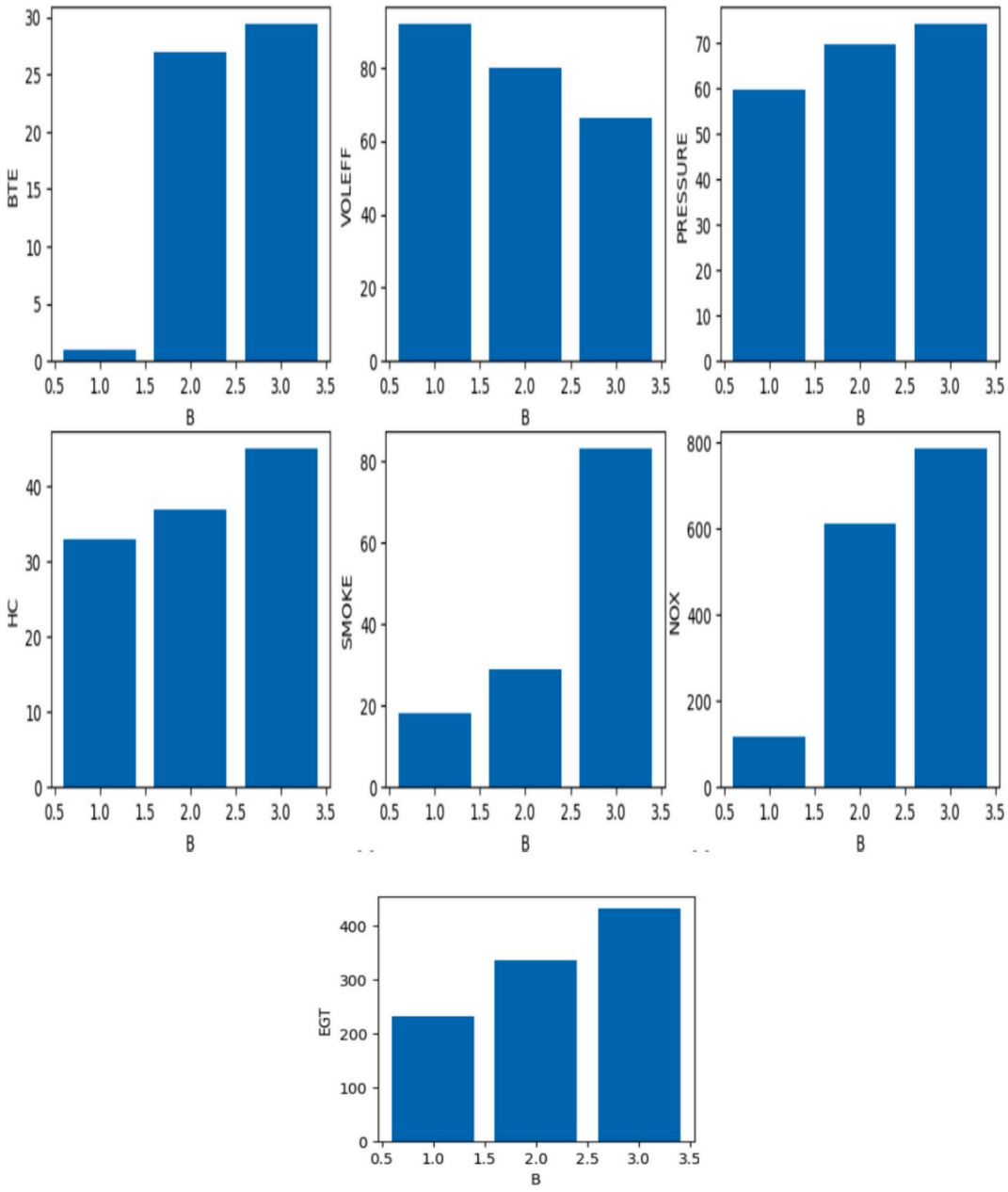

Fig. 40. Depicts the interaction between B and the other related factors.

8. Python-driven evaluation of input–output interactions in engine systems

Pham et al. [38] emphasize Python as a versatile scripting language collaboratively established by multiple contributors to address complex issues in Multicriteria managerial (MCDM). Python's widespread adoption among programmers is largely attributed to its readability, straightforward syntax, and open-source availability, which enable its application across diverse fields. Leveraging Python's extensive libraries, MCDM frameworks can systematically evaluate dependable options and streamline decision-making workflows, minimizing reliance on expert judgment. Specifically, in diesel engine research, Python serves as a powerful tool for evaluating engine performance metrics, optimizing fuel consumption, and mitigating pollutant emissions. This investigation utilizes Python to explore and quantify the interactions between engine input variables and their resulting output characteristics.

9. Statistical mapping of engine input factors to output behaviors

This segment applies detailed statistical examination to investigate the complex relationships among input variables A (fuel blend type), B (injection pressures: 170, 200, 230 bar), and C (engine load levels: no load, partial load, full load) alongside various output metrics. The output parameters analyzed include smoke opacity, cylinder loading, exhaustive vapor temperature (EGT), brake thermal efficacy (BTE), brake specified energy utilization (BSEC), volumetric efficacy, and emission levels of hydrocarbons (HC), carbon monoxide (CO), and nitrogen oxides (NOx). Utilizing Python's library, a correlation matrix was carefully constructed to quantify the intensity and direction of linear associations: coefficients approaching $+1$ denote a strong direct relationship, values near -1 indicate a strong inverse association, and those close to zero reflect negligible or no linear connection whatsoever. The findings reveal that injection pressure (input B) notably affects multiple

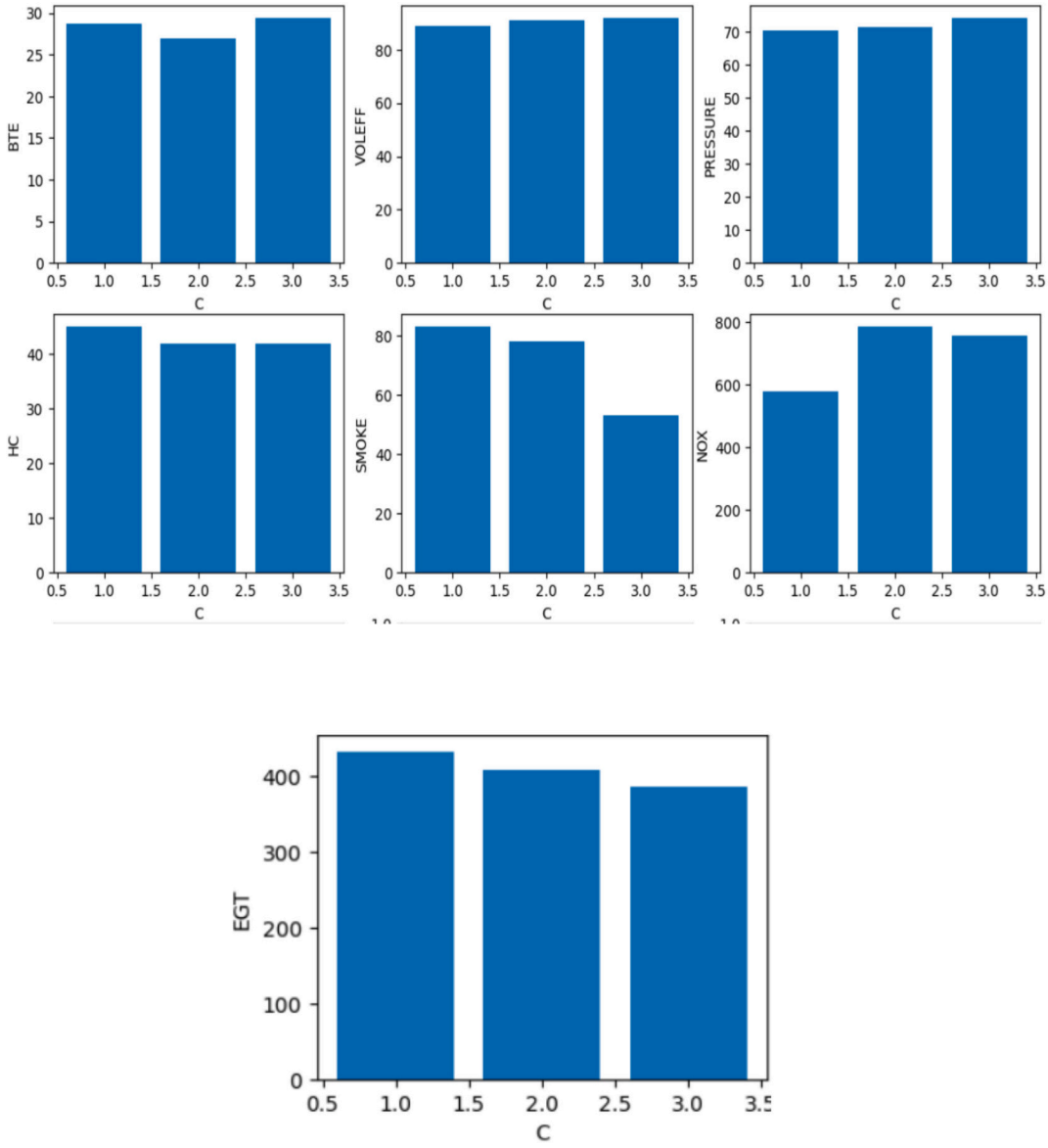

Fig. 41. Depicts the interaction between C and the other related factors.

important output characteristics such as BTE, volumetric efficiency, cylinder pressure, HC, smoke, NOx, EGT, and BSEC. Notably, volumetric efficiency exhibits an inverse correlation with injection pressure, implying that increased injection pressure corresponds with a noticeable decline in volumetric efficiency. A comprehensive summary of these correlations between the input factors and experimental responses is presented in Table 9 for clear reference.

The examined output variables demonstrated minimal dependency on the input factor identified as blend type, labeled A. Negative correlations appeared for brake thermal efficacy (BTE), volumetric efficacy, cylinder loading, and carbon monoxide (CO) emissions, though these values did not approach strong inverse thresholds near −1. This indicates that these outputs have a subtle inverse linkage with the proportion of pyrolysis oil in the blend. Specifically, elevating the pyrolysis oil fraction tends to slightly reduce these metrics, while lowering it produces the reverse effect. Conversely, the remaining output parameters showed positive correlations with blend type A; however, these associations lacked robust statistical validation. This implies that increasing pyrolysis oil content might modestly improve those parameters, but the relationship remains weak and inconclusive.

Injection pressure, denoted as input B, exhibits strong associations with several output metrics. Specifically, brake thermal efficiency (BTE) shows a robust positive correlation (0.913) with rising injection pressure, whereas volumetric efficiency (VOLEFF) demonstrates a pronounced negative correlation (−0.993). Additionally, parameters such as cylinder pressure (0.898), hydrocarbon emissions (0.825), smoke opacity (0.884), nitrogen oxides (NOx) concentration (0.941), and exhaust gas temperature (EGT) (0.970) tend to increase in tandem with higher injection pressures. Brake specific energy consumption (BSEC) reveals a moderate positive linkage (0.753). In contrast, the engine load (input C) presents comparatively weaker correlations with cylinder pressure (0.268) and NOx (0.232), while exerting minimal influence over other output variables. The blend composition (input A) alongside load (C) generally exerts negligible effects on most measured outputs. These patterns are graphically illustrated in Figs. 39, 40, and 41, corresponding to inputs A, B, and C, respectively. Overall, the analysis underscores injection pressure as the dominant factor shaping output characteristics, with blend type and engine load having only limited impacts [54–56].

10. Summative insights and key findings

This study evaluated the performance, combustion, and emission characteristics of CI engines using ternary blends of biodiesel, pyrolysis oil, and diesel under varying injection pressures. The key findings are summarized as follows:

- Optimal injection pressure: 230 bar yielded the best results, improving brake thermal efficiency (BTE), air–fuel mixing, and combustion effectiveness.
- Blend performance: Biodiesel blend set 2 (P10B220D70, P15B215D70, P5B225D70) showed lower fuel consumption and better thermal behavior due to balanced fuel properties.
- Volumetric efficiency: Increased with higher injection pressure due to better air intake and atomization; it dropped at lower pressures due to incomplete combustion and exhaust retention.
- Exhaust gas temperature (EGT): Rose with injection pressure across all blends, indicating higher in-cylinder heat release.
- Combustion behavior: Biodiesel blends exhibited higher heat release rates (HRR), with sample 3 peaking at 66.55 kJ/m^3.°CA, enhancing combustion quality.
- Cylinder pressure: Peak values reached up to 70.5 bar with certain blends at 230 bar; however, extreme pressure variations affected spray characteristics and peak pressure.
- Emissions: P15B blends had higher NOx emissions, while P5B blends emitted less due to slower combustion. CO emissions reduced slightly at higher pressures due to better atomization.
- Parameter sensitivity: Injection pressure had the strongest influence on performance and emissions. Blend composition and engine load had minor effects comparatively.

CRediT authorship contribution statement

J. Mohammed Azarudeen: Project administration. **Anish Mariadhas:** Conceptualization. **Jayaprabakar Jayaraman:** Data curation. **S. Yashashwini:** Formal analysis. **A. Vivek Anand:** Investigation. **Karthick Muniyappan:** Methodology. **Ankur Bahl:** Project administration. **Mohammad Kanan:** Resources. **R. Muraliraja:** Validation. **Vimal Ramanathan:** Visualization.

Declaration of competing interest

The authors declare that they have no known competing financial interests or personal relationships that could have appeared to influence the work reported in this paper.

Data availability

Data will be made available on request.

References

[1] H. Hosseinzadeh-Bandbafha, A.S. Nizami, S.A. Kalogirou, V.K. Gupta, Y.K. Park, A. Fallahi, M. Tabatabaei, Environmental life cycle assessment of biodiesel production from waste cooking oil: a systematic review, Renew. Sustain. Energy Rev. 161 (2022) 112411.

[2] S.K. Nayak, G.R. Behera, P.C. Mishra, S.K. Sahu, Biodiesel vs diesel: a race for the future, Energy Sources, Part A: Recovery, Utilization, and Environmental Effects 39 (14) (2017) 1453–1460.

[3] S.K. Nayak, P.C. Mishra, A. Kumar, G.R. Behera, B. Nayak, Experimental investigation on property analysis of Karanja oil methyl ester for vehicular usage, Energy Sources, Part A 39 (3) (2017) 306–312.

[4] C. Chen, A. Chitose, M. Kusadokoro, H. Nie, W. Xu, F. Yang, S. Yang, Sustainability and challenges in biodiesel production from waste cooking oil: an advanced bibliometric analysis, Energy Rep. 7 (2021) 4022–4034.

[5] R.M. Mohamed, G.A. Kadry, H.A. Abdel-Samad, M.E. Awad, High operative heterogeneous catalyst in biodiesel production from waste cooking oil, Egypt. J. Pet. 29 (1) (2020) 59–65.

[6] Y. Liu, X. Yang, A. Adamu, Z. Zhu, Economic evaluation and production process simulation of biodiesel production from waste cooking oil, Curr. Res. Green Sustain. Chem. 4 (2021) 100091.

[7] S.K. Nayak, P.C. Mishra, Emission characteristics of diesel fuel composed of linseed oil (Linum Usitatissium) blends utilizing rice husk producer gas, Energy Sources, Part A: Recovery, Utilization, and Environmental Effects 38 (14) (2016) 2001–2008.

[8] L. Rocha-Meneses, A. Hari, A. Inayat, L.A. Yousef, S. Alarab, M. Abdallah, T. Kikas, Recent advances on biodiesel production from waste cooking oil (WCO): a review of reactors, catalysts, and optimization techniques impacting the production, Fuel 348 (2023) 128514.

[9] S.K. Nayak, P.C. Mishra, Emission characteristics of jatropha oil blends using waste wood producer gas, Energy Sources, Part A: Recovery, Utilization, and Environmental Effects 38 (14) (2016) 2153–2160.

[10] S. Banga, V.V. Pathak, Biodiesel production from waste cooking oil: a comprehensive review on the application of heterogenous catalysts, Energy Nexus 10 (2023) 100209.

[11] N. Outili, H. Kerras, C. Nekkab, R. Merouani, A.H. Meniai, Biodiesel production optimization from waste cooking oil using green chemistry metrics, Renew. Energy 145 (2020) 2575–2586.

[12] C. Adhikesavan, D. Ganesh, V.C. Augustin, Effect of quality of waste cooking oil on the properties of biodiesel, engine performance and emissions, Clean. Chem. Eng. 4 (2022) 100070.

[13] M.J. Costa, M.R. Silva, E.E. Ferreira, A.K.F. Carvalho, R.C. Basso, E.B. Pereira, D. B. Hirata, Enzymatic biodiesel production by hydroesterification using waste cooking oil as feedstock, Chem. Eng. Processing-Process Intens. 157 (2020) 108131.

[14] S. Sivarethinamohan, J.R. Hanumanthu, K. Gaddam, G. Ravindiran, A. Alagumalai, Towards sustainable biodiesel production by solar intensification of waste cooking oil and engine parameter assessment studies, Sci. Total Environ. 804 (2022) 150236.

[15] K. Velmurugan, A.P. Sathiyagnanam, Impact of antioxidants on NOx emissions from a mango seed biodiesel powered DI diesel engine, Alex. Eng. J. 55 (1) (2016) 715–722.

[16] A. Sharma, S. Murugan, Potential for using a Tyre pyrolysis oil-biodiesel blend in a diesel engine at different compression ratios, Energy Conver. Manage. 93 (2015) 289–297.

[17] T. Seljak, S.R. Oprešnik, T. Katrašnik, Combustion characteristics of tire pyrolysis oil in turbo charged compression ignition engine, Fuel 150 (2015) 226–235.

[18] A.B. Koc, M. Abdullah, Performance of a 4-cylinder diesel engine running on tire oil–biodiesel–diesel blend, Fuel Process. Technol. 118 (2014) 264–269.

[19] A. Sanyal, A.K. Choudhary, Environmental impact of waste plastic oil and hydrogen-enriched diesel engines: a comprehensive review on performance, combustion, and emissions, J. Renew. Sustain. Energy 16 (5) (2024).

[20] Y. Zhao, C. Wang, L. Zhang, Y. Chang, Y. Hao, Converting waste cooking oil to biodiesel in China: environmental impacts and economic feasibility, Renew. Sustain. Energy Rev. 140 (2021) 110661.

[21] M. Corral-Bobadilla, R. Lostado-Lorza, F. Somovilla-Gómez, S. Íñiguez-Macedo, Life cycle assessment multi-objective optimization for eco-efficient biodiesel production using waste cooking oil, J. Clean. Prod. 359 (2022) 132113.

[22] P. Sambandam, P. Murugesan, V.K. Thangaraj, M. Vadivel, M. Rajaraman, G. Subbiah, Environmental impact of waste plastic pyrolysis oil on insulated piston diesel engine with methoxyethyl acetate additive, Pet. Sci. Technol. 41 (10) (2023) 1113–1130.

[23] V.S. Kharkwal, S. Kesharvani, S. Verma, G. Dwivedi, S. Jain, Numerical investigation of engine characteristics of a diesel engine fuelled with ethanol and diethyl ether supplemented Diesel-WCO biodiesel blend, Mater. Today: Proc. (2023), https://doi.org/10.1016/j.matpr.2023.02.106.

[24] A. Kumar, H.S. Pali, M. Kumar, Evaluation of waste plastic and waste cooking oil as a potential alternative fuel in diesel engine, Next Energy 5 (2024) 100181.

[25] E. Parandi, M. Safaripour, M.H. Abdellattif, M. Saidi, A. Bozorgian, H.R. Nodeh, S. Rezania, Biodiesel production from waste cooking oil using a novel biocatalyst of lipase enzyme immobilized magnetic nanocomposite, Fuel 313 (2022) 123057.

[26] A. Sharma, S. Murugan, Effect of blending waste Tyre derived fuel on oxidation stability of biodiesel and performance and emission studies of a diesel engine, Appl. Therm. Eng. 118 (2017) 365–374.

[27] D.R. Vallapudi, H.K. Makineni, S.K. Pisipaty, H. Venu, Combined impact of EGR and injection pressure in performance improvement and NOx control of a DI diesel engine powered with tamarind seed biodiesel blend, Environ. Sci. Pollut. Res. 25 (2018) 36381–36393.

[28] M.K. Yesilyurt, The effects of the fuel injection pressure on the performance and emission characteristics of a diesel engine fuelled with waste cooking oil biodiesel-diesel blends, Renew. Energy 132 (2019) 649–666.

[29] C.G. Saravanan, K.R. Kiran, M. Vikneswaran, P. Rajakrishnamoorthy, S.P.R. Yadav, Impact of fuel injection pressure on the engine characteristics of CRDI engine powered by pine oil biodiesel blend, Fuel 264 (2020) 116760.

[30] A.K. Srivastava, S.L. Soni, D. Sharma, N.L. Jain, Effect of injection pressure on performance, emission, and combustion characteristics of diesel–acetylene-fuelled single cylinder stationary CI engine, Environ. Sci. Pollut. Res. 25 (2018) 7767–7775.

[31] M. Fırat, Ş. Altun, M. Okcu, Y. Varol, Experimental investigation on combustion and emission characteristics of reactivity controlled compression ignition engine powered with iso-propanol/biodiesel blends, Propuls. Power Res. 11 (2) (2022) 224–239.

[32] E. Elavazhagan, A. Sowmiya, S. Sivalingam, Comprehensive analysis and process simulation of biodiesel production from biomass sources, Ind. J. Chem. Technol. (IJCT) 30 (5) (2023) 623–633.
[33] P. Jena, R. Raj, J.V. Tirkey, A. Kumar, Experimental analysis and optimization of CI engine performance using waste plastic oil and diesel fuel blends, J. Energy Inst. 109 (2023) 101286.
[34] K. Yeneneh, G. Sufe, Enhancing diesel engine performance and emissions using alumina nanoparticle-blended waste plastic oil biodiesel: an experimental and predictive approach, Indust. Eng. Chem. Res. 64 (24) (2025) 11681–11694.
[35] S.P. Sundar, P. Vijayabalan, R. Sathyamurthy, Z. Said, A.K. Thakur, Experimental and feasibility study on nano blended waste plastic oil based diesel engine at various injection pressure: a value addition for disposed plastic food containers, Fuel Process. Technol. 242 (2023) 107627.
[36] S.N. Gopan, A.V. Rajan, B.R. Krishnan, Review of bio-diesel production from waste cooking oil and analyze the IC engine performance, Mater Today Proc 37 (2021) 1208–1211.
[37] J. Jayaraman, K. Alagu, C.J. Raorane, P. Appavu, N. Joy, A. Mariadhas, M. Rajasimman, Zinc oxide nanoparticles to the synthesis of high-value added biofuels from waste cooking oil methyl ester blends, Fuel 332 (2023) 126170.
[38] E.C. Pham, D. Van Nguyen, Optimization of ultrasound-assisted biodiesel production from python fat oil using response surface methodology, Energy Nexus 16 (2024) 100331.